Phase-space organizations in prolate and oblate potentials: Classical, semiclassical, and quantum results

R. Arvieu, F. Brut, and J. Carbonell
Institut des Sciences Nucléaires, F-38026 Grenoble-Cédex, France

J. Touchard
Division de Physique Théorique, Institut de Physique Nucléaire, F-91406, Orsay-Cédex, France
(Received 22 July 1986)

The three-dimensional trajectories of a neutron in an average deformed potential are studied for two different potentials with prolate or oblate ellipsoidal deformations. The simplest one is a simple cavity which is shown to be integrable. The motion is studied and is found to be separable in spheroidal coordinates. It is shown that the phase space of an oblate cavity may contain a separatrix which is associated with the crossing of the focal circle while the prolate phase space does contain a separatrix only for the planar trajectories. By using arguments based on a uniform semiclassical approximation, it is shown that the quantum-energy-level spectra present indeed a difference between prolate and oblate shapes corresponding to the crossing of this separatrix. The second potential studied, the Buck-Pilt potential, has a diffuse surface. When it is deformed it becomes unintegrable. For this potential Poincaré surfaces of section are drawn. Large regular regions are shown in which the organization of the phase space is that of the cavity. Chaos and nonlinearities are also seen. Consequences of the existence of the regular regions similar to the cavity are drawn for the energy spectrum.

I. INTRODUCTION

This paper deals with the three-dimensional trajectories of a particle in an axially symmetric potential with an ellipsoidal deformation. Our aim is to discuss the organization of the classical phase space for a problem which has a quantum analogue mainly used in the description of deformed nuclei. In previous papers we have already studied the planar trajectories. In Carbonell *et al.*[1] attention was concentrated on the case of spherically symmetric potentials, and in Ayant and Arvieu[2,3] on the trajectories lying in meridian planes of deformed potentials. In these papers semiclassical quantization was performed by using the Einstein-Brillouin-Kramers (or EBK) method; in Refs. 2 and 3 the role of the uniform approximation was particularly underlined. In the present paper we will consider in a first step an ellipsoidal box with a sharp surface and a cavity, and in a second step an ellipsoidally deformed version of a diffuse nuclear average potential called the Buck-Pilt,[4] or BP, potential. We will consider here only the effects which come out from the purely central nuclear part; Coulomb force, pairing effects, and the inertial forces due to the rotation of the potential will not be treated.

We intend to discuss three points. First we want to sketch the organization of the phase space for nonplanar trajectories. Because of axial symmetry the angular-momentum projection L_z on this axis is a constant of motion. It is then sufficient to study the motion in a meridian plane which rotates with the particle around the symmetry axis. Our phase space is therefore simply four dimensional. Secondly, we will underline the main differences between prolate and oblate symmetry. Thirdly, we want to compare the phase spaces of the BP potential, a nonintegrable potential, with that of the cavity, which is integrable, and we will discuss the occurrence of chaotic trajectories in the former. The two potentials will not be treated on the same footing. The cavity is treated rigorously in an analytic way. The numerical work done there is given only as an illustration. There are no analytical results for the BP potential on the other hand; our work is then entirely numerical. We have drawn a number of trajectories which provide a "reasonably dense" exploration of the phase space. What happens at a finer scale will not be discussed in detail.

The difference between prolate and oblate symmetry is well understood for the cavity. This difference comes into sight if one considers the possibility of focalization of rays for each symmetry. In the prolate case the foci stand on the symmetry axis and the trajectories which cross the foci are contained in meridian plane; they are limited to $L_z=0$. The trajectories with $L_z\neq 0$ have no possibility of focalization. Trajectories which focalize are seen to stand on a separatrix. Because of the absence of a separatrix the phase space of $L_z\neq 0$ trajectories is made in one piece. On the contrary, the foci are replaced in the oblate shape by a focal circle which stands in the equatorial plane. This focal circle can be attained by trajectories with any L_z. Under the present circumstances, these trajectories stand on a separatrix. Therefore the phase space of trajectories with arbitrary L_z may contain two pieces for the oblate symmetry. The effect can be explained as well by a constant of motion specific to the symmetry. By using the uniform approximation[2] in order to perform a semiclassical quantization, it can then be deduced that the splitting of the single-particle levels is not performed in the same way for prolate and for oblate shapes. This fact was unknown up to this point under such simple terms.

Since the pioneering works of Contopoulos[5] and of Henon and Heiles[6] on nonlinear dynamics, it is a well-known fact that the addition of a perturbation to an integrable Hamiltonian destroys its integrability. Comparing the deformed BP potential to the deformed cavity, the perturbation appears as a combination of deformation with surface diffuseness. None of this effect indeed, acting alone, is able to produce a nonintegrable potential. A spherical BP potential with surface diffuseness is integrable[1] as well as an ellipsoidally deformed cavity (see later in this paper). It is only when one combines them that the rich organization of phase space, which is well known for generic nonintegrable systems (see, for example, Lichtenberg and Lieberman[7]), is coming out. Since the BP potential for a heavy nucleus is very flat in the interior, it is reasonable to expect a similarity of its phase space with that of the cavity if the nonlinearities are minimized. Thus the cavity provides a useful "skeleton" for describing the organization of the phase space of the BP potential. However for appropriate deformations and symmetry, and for specific initial conditions, the nonlinearities are expected to take over, the most spectacular signature being the generation of chaotic trajectories. In the following we will indeed show the two aspects of the deformed BP potential: a regular region where its phase space shares much resemblance with that of the cavity and an irregular one where the nonlinearity takes over. We will show that the second case, i.e., the production of macroscopic chaos in a large part of the phase space, need oblate rather than prolate shapes, large deformation, small L_z, and small binding energy. These conditions justify that the skeleton provided by the cavity can be used rather extensively and provides a basis to explain the important similarity, observed for heavy nuclei, between the single-particle spectrum of the BP deformed potential and that of the cavity.

A preliminary discussion of the organization of the phase space for oblate and prolate cavities has already been given in Ref. 8. The description of the phase space of the planar trajectories ($L_z=0$) of the deformed BP potential has been given by Carbonell.[9] The topological flow in phase space that is simply sketched in the present paper is more carefully done in Ref. 9 for the $L_z=0$ case (see also Ref.10).

II. THE ELLIPSOIDAL CAVITY

In the following we will examine the various species of trajectories which correspond to the motion of a free particle in a cavity of ellipsoidal shape with axial symmetry. The cavity, assumed to be not rotating or vibrating, acts as a perfect reflector. The difference between the prolate and the oblate symmetries is of primary importance. This difference originates from the existence of two focal points on the axis of symmetry (assumed to be the z axis) in the prolate case and, on the other hand, of a focal circle in the equatorial plane for the oblate one. The possibility of focalization leads to a division of the phase space into two parts. It will be seen later on that this division is a general feature in the oblate case, whatever the value of L_z, the projection of the angular momentum on the axis of symmetry. On the contrary, in the prolate case, focalization is possible only for the planar $L_z=0$ trajectories by symmetry consideration and does not affect the $L_z\neq 0$ phase space. This difference also comes out from a discussion of the special constants of motion that are conserved for each symmetry. It can be equally understood in terms of the effective potentials that appear in appropriate systems of coordinates.

A. Classical description of the prolate case

Although a trajectory in the cavity is composed of a succession of simple segments of straight lines, it is not easy to figure out that each trajectory has an envelope (or a caustic). These caustics are found in a system of coordinates in which the motion is separable. These systems are the spheroidal coordinates used by Strutinsky *et al.*[11] and in Ref. 2.

In the prolate case let us introduce the spheroidal prolate coordinates; ϵ, ξ, φ, $0\le\epsilon<\infty$, $0\le\xi<\pi$, $0\le\varphi<2\pi$,

$$x=f\sinh\epsilon\sin\xi\cos\varphi\ , \tag{1}$$

$$y=f\sinh\epsilon\sin\xi\sin\varphi\ , \tag{2}$$

$$z=f\cosh\epsilon\cos\xi\ , \tag{3}$$

where $2f$ is the focal distance of the cavity.

After studying the equations of motion,[11] one can easily express the canonical momenta p_ϵ (p_ξ) as a function of ϵ (or, respectively, ξ) and of $p_\varphi=L_z$ as well as E, the separation constant, and kf. The energy W of the particle is written $W=k^2/2m$. The expressions are

$$p_\epsilon^2=k^2f^2\cosh^2\epsilon-\frac{p_\varphi^2}{\sinh^2\epsilon}-E\ , \tag{4}$$

$$p_\xi^2=E-k^2f^2\cos^2\xi-\frac{p_\varphi^2}{\sin^2\xi}\ . \tag{5}$$

They allow us to define the effective potentials $f_P(\epsilon)$ and $g_P(\xi)$ that are seen by each variable by the relations

$$f_P(\epsilon)=k^2f^2\cosh^2\epsilon-\frac{p_\varphi^2}{\sinh^2\epsilon}\ , \tag{6}$$

$$g_P(\xi)=k^2f^2\cos^2\xi+\frac{p_\varphi^2}{\sin^2\xi}\ . \tag{7}$$

Those functions are plotted in Fig. 1 for $kf=1$ and various values of p_φ. The function $f_P(\epsilon)$ is monotonously increasing with ϵ. For a given E the allowed domain of value of ϵ has a lower bound ϵ_0, the turning point $[p_\epsilon(\epsilon_0)=0]$, and an upper value ϵ_1 corresponding to the boundary ($R_z=f\cosh\epsilon_1$). Thus there is always an ellipsoidal caustic, defined by $\epsilon=\epsilon_0$, homofocal to the boundary.

The function $g_P(\xi)$ has a single maximum for $\xi=\pi/2$. This point corresponds to the lowest value of E

$$\inf E=p_\varphi^2 \tag{8}$$

while the upper value of E is given by

$$\sup E=k^2f^2\cosh^2\epsilon_1-\frac{p_\varphi^2}{\sinh^2\epsilon_1}\ . \tag{9}$$

The effective potential $g_P(\xi)$ is symmetric with respect to $\xi=\pi/2$. For every E there are two turning points: ξ' and $\pi-\xi'$, where $p_\xi=0$, which define the two sheets of an hyperboloid of revolution homofocal to the boundary.

The centrifugal effect produces one specific term for each variable. Neighborhoods of $\epsilon=0$, as well as of $\xi=0$ and π, are forbidden. This explains the two caustics. The domain of variation of E, the location of ϵ_0, ϵ_1, and ξ' are shown in Fig. 1 for $p_\varphi^2=0.1$ and an arbitrary ϵ_1. The situation for $p_\varphi=0$ has already been described previously in Ref. 2. There it was seen that we have either one elliptic caustic or an hyperbolic caustic.

It is interesting to remark that for $p_\varphi\neq 0$ we have two interesting limiting trajectories.

(i) For $E=\sup E$ the particle stays on the boundary with $\epsilon=\epsilon_1$ and describes a *geodesic* of the ellipsoid. This geodesic is tangent at two circles defined by the intersection of the hyperboloid caustic corresponding to the proper values of ξ' with the ellipsoidal boundary.

(ii) For $E=\inf E$ the particle is confined in the equatorial plane. Its motion reduces to that of a single particle in a two-dimensional circular "billiard."

Since everything changes continuously and monotonously with E, kf, and p_φ ($p_\varphi\neq 0$), we can assert that the dynamics of a single particle in a prolate cavity has this monotonous smooth feature. We will show later that there are properties of the quantum spectrum that can also be described in the same way.

The trajectories of a particle can be conveniently represented in cylindrical coordinates. If we keep track only of the ϵ,ξ motion, or of the z,ρ coordinates, the trajectory is represented in a plane by an ensemble of segments of hyperbolas bounded by two caustics: one ellipsis (with $\epsilon=\epsilon_0$) and two branches of an hyperbola (with $\xi=\xi'$ and $\pi=\xi'$). Four different trajectories corresponding to different initial conditions are shown in Fig. 2. One of them has been chosen to provide a trajectory very near from the geodesic.

The separation constant E can be expressed in terms of ϵ, ξ, p_ϵ, and p_ξ after elimination of kf from Eqs. (4) and (5). After a long but straightforward calculation the constant E takes the simple form

$$E=\mathbf{l}_1\cdot\mathbf{l}_2\ , \tag{10}$$

where $\mathbf{l}_1$ and $\mathbf{l}_2$ denote the angular momentum with respect to each focus. By using (8) we obtain the condition, for $p_\varphi\neq 0$,

$$\mathbf{l}_1\cdot\mathbf{l}_2>0\ . \tag{11}$$

This expression of the constant of motion generalizes that found for the $p_\varphi=0$ case. However in the latter case the sign of $\mathbf{l}_1\cdot\mathbf{l}_2$ can be positive or negative; this provides a simple classification of the caustics. The case with $p_\varphi=0$ corresponds to the separatrix which has been studied extensively in Ref. 3. The fact that $\mathbf{l}_1\cdot\mathbf{l}_2$ is always positive in a prolate cavity for $p_\varphi\neq 0$ can be associated to the existence of a single type of motion for this type of symmetry. The constant of motion used here belongs to a general class which apply to problems with cylinder symmetry discussed by Helfrich[12] (see also Ref. 13).

B. Classical description of the oblate case

The oblate spheroidal system of coordinates appropriate to that case is simply deduced from the definitions (1)—(3) by permuting $\cosh\epsilon$ with $\sinh\epsilon$. This definition brings the points with $\epsilon=0$ in the equatorial plane of the cavity.

The values of p_ϵ and p_ξ are now easily seen to be

$$p_\epsilon^2=k^2f^2\cosh^2\epsilon+\frac{p_\varphi^2}{\cosh^2\epsilon}-E\ , \tag{12}$$

$$p_\xi^2=E-k^2f^2\sin^2\xi-\frac{p_\varphi^2}{\sin^2\xi}\ . \tag{13}$$

The centrifugal effect occurs only for the variable ξ for $\xi=0$ and $\xi=\pi$. It is now necessary to discuss the struc-

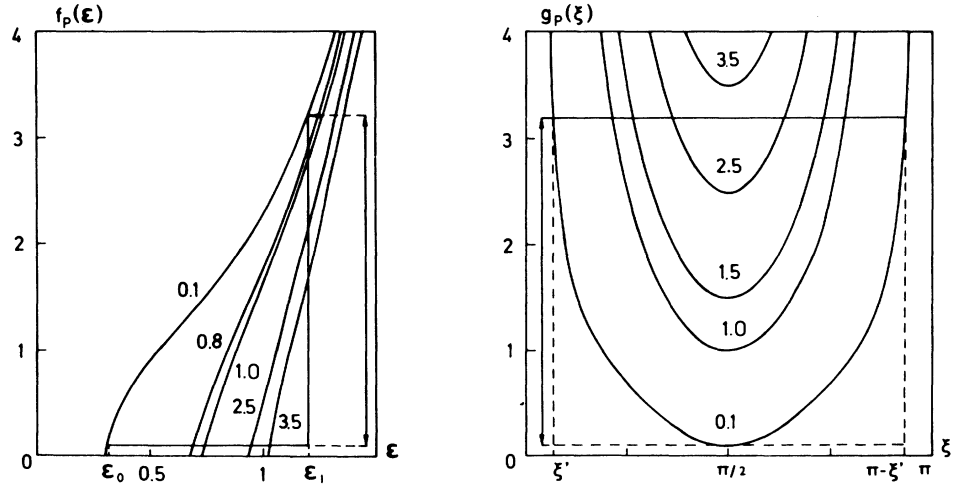

FIG. 1. Left: The effective potential $f_P(\epsilon)$ for the variable ϵ in the prolate case is drawn for $kf=1$ and $p_\varphi^2=0.1,0.8,1.0,2.5,3.5$. The domain of the separation constant E is shown for $p_\varphi^2=0.1$. Right: The effective potential $g_P(\xi)$ for the variable ξ in the prolate case. The domain of E is also shown for $p_\varphi^2=0.1$.

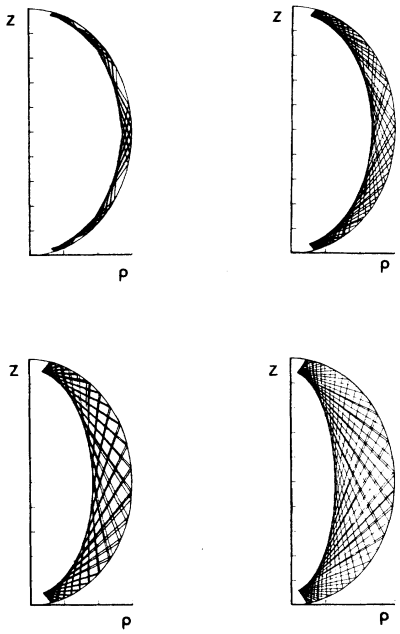

FIG. 2. Some typical trajectories in a prolate cavity with a 2:1 shape and $p_\varphi \neq 0$. The trajectories are represented in the meridian plane of the cavity which rotates with the particle (cylindrical ρ,z coordinates) for four different initial conditions. The upper-left trajectory is not far from a geodesic of the cavity. The units are arbitrary.

ture of the equivalent potentials $f_0(\epsilon)$ and $g_0(\xi)$ defined by

$$f_0(\epsilon)=k^2f^2\cosh^2\epsilon+\frac{p_\varphi^2}{\cosh^2\epsilon}\ , \tag{14}$$

$$g_0(\xi)=k^2f^2\sin^2\xi+\frac{p_\varphi^2}{\sin^2\xi}\ . \tag{15}$$

(i) If $kf<p_\varphi$, Fig. 3 shows that $g_0(\xi)$ has a single minimum for $\xi=\pi/2$ while $f_0(\epsilon)$ has a maximum for $\epsilon=0$ and a minimum for some $\epsilon\neq 0$. It is simply seen that the motion is allowed for the values of E limited by

$$\inf E=g_0(\pi/2)=k^2f^2+p_\varphi^2\ , \tag{16}$$

$$\sup E=f_0(\epsilon_1)=k^2f^2\cosh^2\epsilon_1+\frac{p_\varphi^2}{\cosh^2\epsilon_1}\ . \tag{17}$$

The value (16) corresponds to the planar trajectory in the equatorial plane of the ellipsoid, (17) to a geodesic. For $kf<p_\varphi$ there is then one ellipsoidal and one hyperboloidal caustic homofocal to the boundary. The difference with the prolate case stems from the fact that since the focal line lies in the equatorial plane, a one-sheet hyperboloid is enough to avoid crossing the z axis. The domain of E and the associated values of ϵ_1 and ξ' are represented for $p_\varphi^2=1.5$ in Fig. 3.

(ii) If $kf>p_\varphi$, Fig. 3 shows that $g_0(\xi)$ has two minima for $\xi=\xi_0$ and $\xi=\pi-\xi_0$ and a local maximum at $\xi=\pi/2$. On the other hand $f_0(\epsilon)$ is now a monotonously increasing function of ϵ. While the upper limit of E is still given by (17) and still corresponds to the geodesic, the lower limit takes the value

$$\inf E=g_0(\xi_0)=2p_\varphi kf\ . \tag{18}$$

The trajectory which corresponds to this value of E is defined by

$$\xi=\xi_0 \quad \text{for } z>0\ , \tag{19}$$

$$\xi=\pi-\xi_0 \quad \text{for } z<0\ , \tag{20}$$

and

$$0\leq\epsilon\leq\epsilon_1\ . \tag{21}$$

This trajectory is represented in the ϵ,ξ or ρ,z plane of coordinates by one segment of hyperbola limited by the boundary. It is interesting to represent it in three dimensions. Let $z_0=f\sinh\epsilon_1\cos\xi_0$. Since one hyperbola in the ρ,z plane represents a segment of straight line in three di-

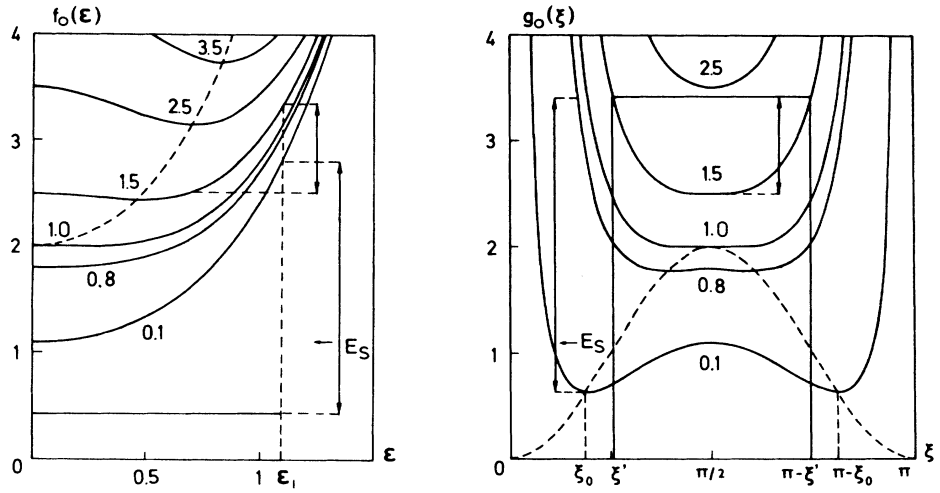

FIG. 3. Effective potentials for the oblate case, $kf=1$, and several values of p_φ^2. The domain of the separation constant E is shown for $p_\varphi^2=0.1$ and 1.5. The loci of the extremum of f_0 and g_0 are represented by a dotted line.

mensions, the curve defined by Eqs. (19)—(21) is made by an ensemble of straight lines, all of the same length, which oscillates between the values $z=+z_0$ and $z=-z_0$ in the same way that a string binding a drum connects alternatively the two parchments (this drum possesses an hyperboloidal side).

The curve $g_0(\xi)$ presents a maximum at $\xi=\pi/2$ which one obtains if

$$E=E_S=k^2f^2+p_\varphi^2 \ . \tag{22}$$

Below this maximum there is a symmetric double well. At the bottom of the well is found the trajectory with $\xi=\xi_0$, $\pi-\xi_0$ defined above.

If $E>E_S$, the caustics are identical to those of the case $kf<p_\varphi$: one ellipsoid and a one-sheet hyperboloid. If $E<E_S$, the ellipsoid disappears and is replaced by a second one-sheet hyperboloid. When $E=\inf E$, the two hyperboloids coalesce and form the curve discussed above for $\xi=\xi_0$ and $\pi=\xi_0$.

For the value $E=E_S$ it can be seen that the trajectory has still an hyperboloidal caustic and the focal circle is the secondary caustic. The separatrix is composed of two pieces: (i) a planar trajectory tangent to the circle with $\rho=f$ (i.e., the trajectory with $\xi=\pi/2$) and (ii) a nonplanar trajectory, with $\xi\neq\pi/2$, which always crosses the equatorial plane at the focal circle.

The situation with $kf>p_\varphi$ is the most interesting for us since we have a subdivision of phase space into two parts and since the effective potential has a change in its topology at $E=E_S$. This transition is a purely geometric one although it has been found here by using classical mechanics. It can be produced for any value of f, k, and p_φ which fulfill the inequality $kf>p_\varphi$.

Trajectories of the oblate case are represented in Fig. 4. We have chosen to fix the deformation of the ellipsoid to a 2:1 shape and to change the initial conditions (and also L_z) in order to show the two topologies.

Finally, in a discussion parallel to that of the prolate case the separation constant can also be expressed by simple quantities. We can show after an identically tedious calculation that E takes the form

$$E=l^2+f^2k_\perp^2 \ , \tag{23}$$

where $k_\perp$ is the projection of the momentum on the equatorial plane and l is the angular momentum. It can also

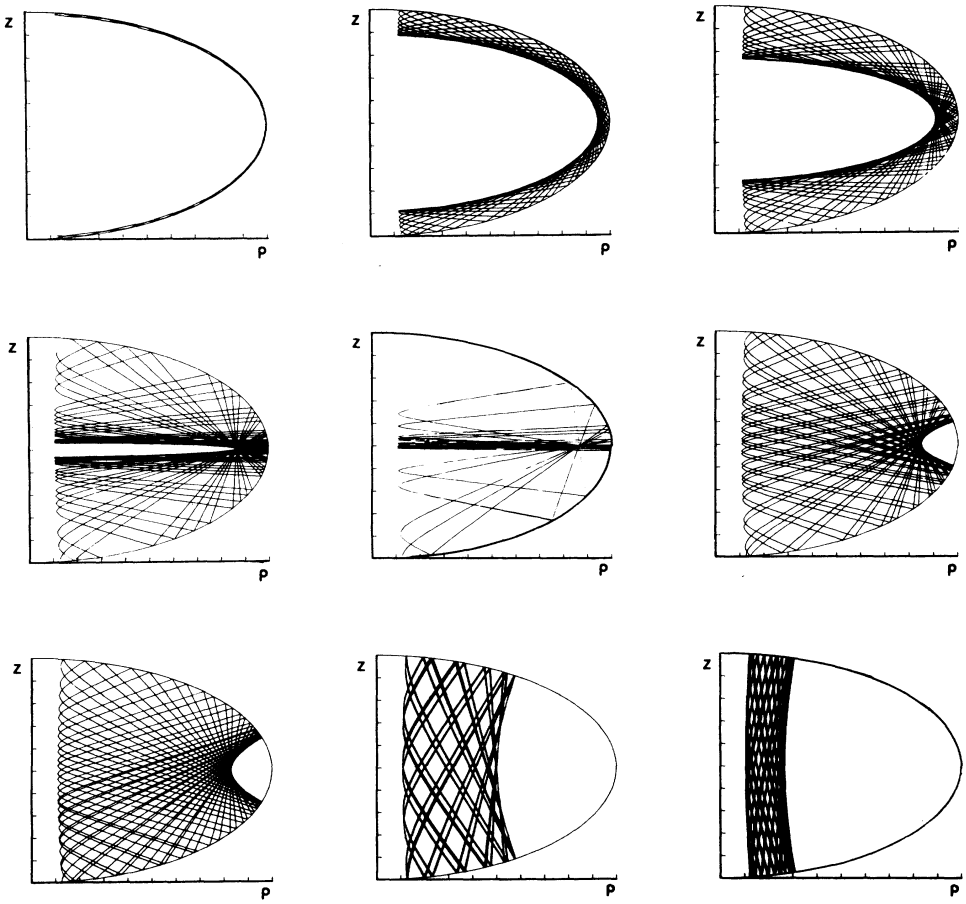

FIG. 4. Some typical trajectories in an oblate cavity with a 2:1 shape and $p_\varphi\neq0$. The representation is the same as in Fig. 2. The upper-left trajectory is also not far from a geodesic; it is the first trajectory with an ellipsoidal caustic. This caustic disappears in the central figure corresponding to the separatrix. The next four trajectories have a hyperboloidal caustic. The bottom-right trajectory is not far from the "string binding a drum" trajectory described in the text.

be written as

$$E=A+l_z^2+f^2k^2=A+E_S\ , \tag{24}$$

where

$$A=l_\perp^2-f^2k_z^2=\mathbf{l}_{1_\perp}\cdot\mathbf{l}_{2_\perp}\ . \tag{25}$$

The conservation of E implies finally the conservation of A defined by Eqs. (25) in terms of $l_\perp$ and k_z or in terms of $\mathbf{l}_{1_\perp}$ and $\mathbf{l}_{2_\perp}$, the projection of $\mathbf{l}_1$ and $\mathbf{l}_2$ on the equatorial plane. Here 1 and 2 denote any opposite points of the focal circle with respect to which are defined the angular momentum $\mathbf{l}_1$ and $\mathbf{l}_2$. The conservation of $A=\mathbf{l}_{1_\perp}\cdot\mathbf{l}_{2_\perp}$ in the oblate case is reminiscent of that of $E=\mathbf{l}_1\cdot\mathbf{l}_2$ for the prolate one.

In terms of A the two topologies are characterized by the sign of A since $A<0$ if $E<E_S$. It is interesting to note the limits of A. If $E>E_S$,

$$0<A\leq k^2R_<^2-p_\varphi^2\frac{R_<^2}{R_>^2}\ . \tag{26}$$

If $E<E_S$,

$$-(kf-p_\varphi)^2\leq A<0\ . \tag{27}$$

In conclusion we have been able to prove that there is an essential difference for $p_\varphi\neq 0$ between the phase space of an oblate ellipsoidal cavity and the phase space of a prolate ellipsoidal cavity. While the latter has a monotonous character, the former exhibits a bifurcation at some stage and a division into two parts.

C. Poincaré surfaces of section

Although the discussion of the dynamics of the free particle in the cavity is well understood, it is convenient to add another piece of information on the phase space that will be useful later on in the discussion of our diffuse potential well. The Poincaré surfaces of section are extremely useful tools to illustrate the structure of the phase space and to follow its evolution when some parameters are varied. We define the surfaces of sections in the conventional way[6,7] as follows. Let us calculate the projection p_ρ of the momentum of the particle on the equatorial plane for every intersection ρ of the particle with this plane with $p_z>0$. The surface of section is defined as the set of invariant curves $p_\rho(\rho,kf,E)$ that exists for a given kf and for various values of the separation constant E. In our case this function can be defined analytically and is written simply as

$$p_\rho^2=k^2-\frac{A}{\rho^2\pm f^2}-\frac{p_\varphi^2}{\rho^2}\ . \tag{28}$$

The constant of motion A is written here in the form

$$A=l_\perp^2\pm f^2k^2\ . \tag{29}$$

The signs + and − correspond to prolate and oblate ellipsoids, respectively. The curves $p_\rho(\rho)$ for various A are plotted in Fig. 5 for $kf<p_\varphi$ and $kf>p_\varphi$. The geodesic is represented by the point $p_\rho=0$ with $\rho=\rho_{\max}$, the boundary of the surface of section, as the curve with the lowest possible value of A, i.e., the planar trajectory at the equator. It is not a surprise to see the division of the phase space into two domains in the oblate case for $kf>p_\varphi$.

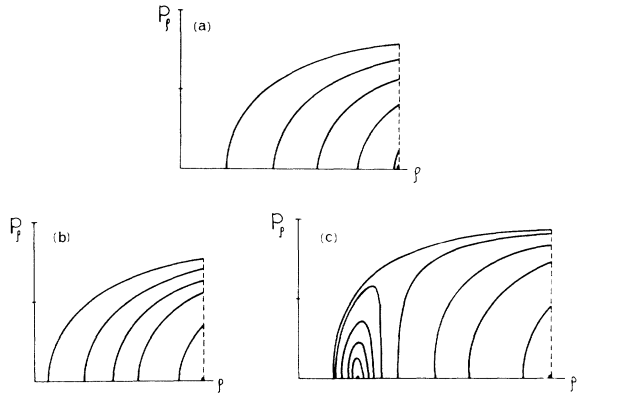

FIG. 5. Poincaré surfaces of section (ρ,p_ρ) of the ellipsoidal cavity. ρ and p_ρ (greater than 0) are drawn in arbitrary units for: (a) a prolate cavity with $p_\varphi/kf=1$, (b) an oblate cavity with $(p_\varphi/kf)^2=2.5$, and (c) an oblate cavity with $(p_\varphi/kf)^2=0.5$. In each section the energy of the particle, the deformation, and the values of p_φ are fixed. Change of the initial conditions provides different values of E or A, hence different curves. The fixed points of the mappings correspond to stable periodic trajectories: the geodesic is found at the maximum value of ρ. In the oblate case the new topology appears on the left of the mapping in (c); it is organized around a "string around the drum" stable trajectory for a low value of ρ.

III. SEMICLASSICAL DESCRIPTION OF THE CAVITY

On the basis of the description performed previously on the cavity eigenstates with $L_z=0$, it is interesting to use semiclassical method in order to draw all the consequences about the spectrum of oblate and prolate shapes for $L_z\neq 0$.

A. Separation of variables of the wave equation

It has already been shown[2] that the wave equation is also separable in spheroidal prolate and oblate systems of coordinates. The only change with respect to classical mechanics that should be taken into account is to replace p_φ^2 in the equivalent potential by $p_\varphi^2-\frac{1}{4}$ in all the expressions giving p_ϵ and p_ξ. Similarly the separation constant should be replaced by $E+\frac{1}{4}$. Thus for $p_\varphi>\frac{1}{2}$ the centrifugal terms in the wave equations have the same sign as in the classical case. For $p_\varphi=0$ those terms become centripetal and their effect has already been studied. Since the effective potentials for $p_\varphi>1/2$ have the same shape as in Sec. II, we can discuss the effect of the symmetry of the potential on the WKB phases on the consideration of Figs. 1 and 2 using arguments developed in Ref. 2.

B. Prolate case

The equivalent potential $f_P(\epsilon)$ is a monotonously increasing function of ϵ which can be most often approxi-

mated by a linear function. On the other hand $g_P(\xi)$ represents a smooth, symmetric, and rather harmonic potential well. In both cases there is no particular need to use the uniform approximation for the WKB phases for any value of $p_\varphi > \frac{1}{2}$. If ϵ_0, ξ_0, and $\pi-\xi_0$ denote the turning points, the action integrals are defined as

$$I_\epsilon = \frac{1}{\pi}\int_{\epsilon_0}^{\epsilon} p_\epsilon d\epsilon \ , \tag{30}$$

$$I_\xi = \frac{1}{\pi}\int_{\xi_0}^{\pi-\xi_0} p_\xi d\xi \ . \tag{31}$$

The WKB or EBK quantization conditions are now written in units $\hbar=1$:

$$I_\epsilon = n_\epsilon + \tfrac{3}{4} = n + \tfrac{3}{4} \ , \tag{32}$$

$$I_\xi = n_\xi + \tfrac{1}{2} = l - |m| + \tfrac{1}{2} \ . \tag{33}$$

The Maslov's indices $\frac{3}{4}$ and $\frac{1}{2}$ are taken from the primitive WKB approximation. In a uniform approximation, which is not attempted here, these numbers should be replaced by smoothly varying functions which should not go much apart from $\frac{3}{4}$ and $\frac{1}{2}$ as was proved for $p_\varphi=0$.

The quantum numbers associated with each variable are identified to the quantum numbers of the radial and azimuthal motion, respectively, for the variable ϵ and ξ. Indeed in the limit where the cavity becomes spherical the motion described by ϵ becomes identical to the radial motion and that described by ξ to the azimuthal motion. It is known in classical mechanics that the azimuthal action I_θ is written (see Ref. 14, p. 473) in terms of the angular momentum and its projection m as

$$I_\theta = l - |m| \tag{34}$$

which justifies formula (33).

Since the effective potentials f_P and g_P change smoothly with kf or p_φ, we also expect a smooth change of the WKB eigenvalues with deformation for a prolate shape. No particularly systematic difference is expected between even m and odd m. Section IV will provide a full justification of this assertion.

C. Oblate case

The existence of potential barriers with variable topology for ϵ as well as for ξ is specific to this case. A particular discussion of the WKB phases is needed which implements that already given for $L_z=0$. Let us remember that the total wave function should be even or odd with respect to σ_h: the reflection operator with respect to the equatorial plane, i.e., to the replacement $\xi \to \pi-\xi$. It is well known[15] and we have redone the demonstration in Ref. 2, that the semiclassical approximation is largely improved if the WKB phase is changed continuously when the energy level crosses the top of a barrier. This change is calculated with the help of the asymptotic limit of the solutions of the parabolic cylinder equation. It is done[2] in terms of two functions $\beta_S(\alpha)$ and $\beta_A(\alpha)$ which are, respectively, the phases of the even and of the odd wave functions. For the value of E given by

$$E_0 = k^2f^2 + p_\varphi^2 - \tfrac{1}{2} \ , \tag{35}$$

the function $g_0(\xi)$ has a maximum for $k^2f^2 > p_\varphi^2 - \frac{1}{4}$.

The parameter α which measures how far one is from the top of the barrier is

$$\alpha = \frac{E_0 - E}{2(k^2f^2 + p_\varphi^2 - \frac{1}{4})^{1/2}} \ . \tag{36}$$

The phases β are now the same as derived previously[2]

$$\beta_S(\alpha) = \theta - \frac{\pi}{4} + \frac{\alpha}{2}\ln|\alpha| - \frac{\alpha}{2} - \tfrac{1}{2}\arg[(-\tfrac{1}{2}+i\alpha)!] \ , \tag{37}$$

$$\theta = \arctan[(1+e^{2\pi\alpha})^{1/2} + e^{\pi\alpha}] \ , \tag{38}$$

while $\beta_A(\alpha)$ is such that

$$\beta_A(\alpha) = \beta_S(\alpha) + \pi - 2\theta \ . \tag{39}$$

The curves drawn for β_S and β_A in Ref. 2 show the following.

(i) When $\alpha \to -\infty$, i.e., $E > E_S$ (the domain where there is one hyperboloidal and one ellipsoidal caustics),

$$\beta_S \Longrightarrow 0, \quad \beta_A \Longrightarrow \frac{\pi}{2} \ . \tag{40}$$

If $\alpha=0$,

$$\beta_S = \frac{\pi}{8}, \quad \beta_A = \frac{3\pi}{8} \ . \tag{41}$$

(ii) When $\alpha \to \infty$, i.e., $E < E_S$ (the ellipsoidal caustics is then replaced by a second hyperboloid),

$$\beta_S \Longrightarrow \frac{\pi}{4}, \quad \beta_A \Longrightarrow \frac{\pi}{4} \ . \tag{42}$$

In the neighborhood of the $0z$ axis the motion for the variable ξ has one turning point in a region where the potential increases uniformly. It is therefore not necessary to change the WKB phase in that region and the value $-\pi/4$ can be taken. The quantization condition is now written using also Eq. (85) of Ref. 2:

$$I_\xi = \frac{2}{\pi}\int_{\xi_{0<}}^{\xi_{0>}} p_\xi d_\xi = 2\left[n_\xi + \frac{\beta}{\pi} + \tfrac{1}{4}\right] \ . \tag{43}$$

$\xi_{0<}$ is the lowest turning point, and $\xi_{0>}=\pi/2$ if $E > E_S$, or is the second lowest turning point if $E < E_S$. When $\alpha \to -\infty$, the topology is the same as that found for a spherical situation. This limit helps to express n_ξ in terms of the combination $l-|m|$ found for the azimuthal action, as for the prolate case.

For states even under σ_h we obtain

$$I_\xi = 2(n_\xi + \tfrac{1}{4}) = l - |m| + \tfrac{1}{2} \tag{44}$$

(i.e., for $l-|m|$ even). For states odd under σ_h we can also write

$$I_\xi = 2(n_\xi + \tfrac{3}{4}) = l - |m| + \tfrac{1}{2} \tag{45}$$

(i.e., for $l-|m|$ odd).

On the separatrix the even states are quantized with the rule

$$I_\xi = 2(n_\xi + \tfrac{1}{4} + \tfrac{1}{8}) \ , \tag{46}$$

which we write

$$I_\xi = l - |m| + \tfrac{3}{4} , \tag{47}$$

and similarly for $l-|m|$ odd we obtain

$$I_\xi = 2(n_\xi + \tfrac{1}{4} + \tfrac{3}{8}) , \tag{48}$$

which we rewrite

$$I_\xi = l - |m| + \tfrac{1}{4} . \tag{49}$$

In the limit $\alpha \to \infty$ the topology has been changed. However, we keep the same value to the quantum numbers and the condition of quantization becomes

$$I = 2(n_\xi + \tfrac{1}{4} + \tfrac{1}{4}) = l - |m| + 1 \quad \text{for even } l-|m| , \tag{50}$$

$$I = 2(n_\xi + \tfrac{1}{4} + \tfrac{1}{4}) = l - |m| \quad \text{for odd } l-|m| . \tag{51}$$

The variation in the action space due to the change of topology is

$$\Delta I_\xi = \tfrac{1}{2} \quad \text{for even } l-|m| , \tag{52}$$

$$\Delta I_\xi = -\tfrac{1}{2} \quad \text{for odd } l-|m| . \tag{53}$$

For the variable ϵ the function $f_0(\epsilon)$ has a minimum if $kf < (p_\varphi^2 - \frac{1}{4})^{1/2}$ for a value $\bar{\epsilon}$ given by

$$\cosh^4 \bar{\epsilon} = \frac{p_\varphi^2 - \frac{1}{4}}{k^2 f^2} , \tag{54}$$

$$f_0(\bar{\epsilon}) = 2kf(p_\varphi^2 - \tfrac{1}{4})^{1/2} . \tag{55}$$

Note that

$$f_0(0) = k^2 f^2 + p_\varphi^2 - \tfrac{1}{4} , \tag{56}$$

and E should be such that

$$E + \tfrac{1}{4} > k^2 f^2 + p_\varphi^2 - \tfrac{1}{4} > 2kf(p_\varphi^2 - \tfrac{1}{4})^{1/2} . \tag{57}$$

The effective potential is then reasonably approximated by a parabola and we obtain again the parabolic cylinder equation and the corresponding phases. In the same way as for $p_\varphi = 0$ we assert that for all motions with a turning point ϵ_0, i.e., for $E > E_S$, we have the phases

$$\beta_S = \frac{\pi}{4}, \quad \beta_A = \frac{\pi}{4} .$$

The quantization condition can now be formulated as

$$I_\epsilon = n_\epsilon + \tfrac{3}{4} = n + \tfrac{3}{4} . \tag{58}$$

When $kf > (p_\varphi^2 - \frac{1}{4})^{1/2}$, the parabola is now centered at $\epsilon = 0$ and the above condition still holds for $E > E_S$. If $E < E_S$, the other limit should be taken and we get

$$I_\epsilon = n + \tfrac{1}{2} \quad \text{for even states} , \tag{59}$$

$$= n + 1 \quad \text{for odd states} . \tag{60}$$

In the same way as for the variable ξ we expect on the separatrix the rule

$$I_\epsilon = n + \tfrac{5}{8} \quad \text{for the even states} , \tag{61}$$

$$= n + \tfrac{7}{8} \quad \text{for the odd states} . \tag{62}$$

There is a slight difficulty in this discussion when $k^2 f^2 = p_\varphi^2 - \frac{1}{4}$. There the potential is not simply quadratic at the origin but quartic and there is no possibility to use the parabolic cylinder equation and the corresponding WKB phases.

D. The slipping of the action cells

Thus the crossing of the potential barrier introduces also a slipping of the action I_ϵ when E goes from $+\infty$ to $-\infty$ which is

$$\Delta I_\epsilon = -\tfrac{1}{4} \quad \text{for even } l-|m| \text{ states} , \tag{63}$$

$$\Delta I_\epsilon = +\tfrac{1}{4} \quad \text{for odd } l-|m| \text{ states} . \tag{64}$$

This slipping of the phase-space cell generalizes to all values of $l-|m|$ that already found for $m=0$ states in Ref. 2. Because of this slipping the semiclassical spectrum does not vary smoothly when we consider levels with m of opposite parity. Note also that the slipping occurs with the same sign for the even-m components of the even-l multiplets and for the odd-m components of the odd-l ones.

E. Finding the separatrix

It is an interesting question to define the conditions under which a semiclassical eigenstate defined by a set $\{n,l,m\}$ is found on the separatrix. In the case $p_\varphi = 0$ the special values e_S of the eccentricity of the boundary and the value $k_S f$ of kf were shown to be simply given by

$$e_S = \frac{I_\xi}{2I_\epsilon + I_\xi} , \tag{65}$$

$$k_S f = \frac{\pi}{2I_\xi} . \tag{66}$$

For $p_\varphi \neq 0$ new expressions of e_S and $k_S f$ must be found for $E = E_S$. Let

$$I_\xi = \frac{1}{\pi} \int_{\xi_0}^{\pi - \xi_0} p_\xi d\xi . \tag{67}$$

Let us introduce the special value of p_ξ on the separatrix

$$p_\xi = kf(\cos^2\xi - \lambda^2 \mathrm{cotang}^2 \xi)^{1/2} \tag{68}$$

with

$$\lambda = \frac{p_\varphi}{kf} = \sin\xi_0 . \tag{69}$$

An elementary integration enables us to write I_ξ as

$$I_\xi = \frac{2p_\varphi}{\pi} F(\lambda) \tag{70}$$

in terms of a function $F(x)$ defined by

$$F(x) = \frac{(1-x^2)^{1/2}}{x} - \arccos x . \tag{71}$$

Equation (70) replaces, for $p_\varphi \neq 0$, Eq. (66), which allows us to calculate $k_S f$ for $p_\varphi = 0$.

Similarly the action I_ϵ is obtained with the definition

$$I_\epsilon = \frac{1}{\pi} \int_0^{\epsilon_1} p_\epsilon d\epsilon \tag{72}$$

and the special value

$$p_\epsilon = kf(\sinh^2\epsilon - \lambda^2\tanh^2\epsilon)^{1/2} . \quad (73)$$

In the same way the integral is easily calculated. After defining the eccentricity $e_S = (\cosh\epsilon_1)^{-1}$ one obtains the formula

$$I_\epsilon = \frac{p_\varphi}{\pi}[F(\lambda e_S) - F(\lambda)] \quad (74)$$

which can be combined with (70) to give

$$2I_\epsilon + I_\xi = \frac{p_\varphi}{\pi}F(\lambda e_S) \quad (75)$$

and then similarly to (65)

$$\frac{I_\epsilon}{2I_\epsilon + I_\xi} = \frac{2F(\lambda)}{F(\lambda e_S)} . \quad (76)$$

This equation defines the critical eccentricity e_S of the boundary grouping altogether Eqs. (75), (70), and the values of the actions. We find that in every case λe_S is a solution of

$$2I_\epsilon + I_\xi = 2n + l - |m| + 2 = \frac{|m|}{\pi}F(\lambda e_S) , \quad (77)$$

while for even $l - |m|$, λ is a solution of

$$I_\xi = l - |m| + \tfrac{3}{4} = \frac{2|m|}{\pi}F(\lambda) \quad (78)$$

and for odd $l - |m|$, λ is a solution of

$$I_\xi = l - |m| + \tfrac{1}{4} = \frac{2|m|}{\pi}F(\lambda) . \quad (79)$$

For a given multiplet, defined by $\{n,l\}$ these equations define in the (e,kf) plane two curves according to the parity of m. This proves that the splitting of the multiplet is done in a different manner for even m and odd m. We expect therefore a grouping of components of even m on the one hand, and another grouping of components of the opposite parity on the other hand. Since the slipping of the action cell with deformation has an opposite sign [Eqs. (52), (53), (63), and (64)], we expect that the slipping could be visible by varying the deformation and will be clearly seen when the semiclassical states stand on their separatrix. A numerical solution of Eqs. (77), (78), and (79) has been performed and the results are discussed in Sec. III F.

F. Quantum calculations

The aim of this part is to look for a possible track of the structure of phase space found in the preceding sections. We have therefore calculated the spectrum of a deformed cavity for oblate as well prolate shapes. The method used was described in Ref. 2. Typical single-particle orbits $1d$, $3d$, $1h$, and $2g$ are represented in Fig. 6. The energy spectra are measured by the value of $(kR_0)^2$, where R_0 is the radius of the spherical cavity (we assume volume conservation during deformation). They are plotted as a function of the deformation parameter defined, as in our preceding paper,[2] by

$$\mu = \frac{R_>}{R_<} , \quad (80)$$

where $R_>$ and $R_<$ are the semiaxes of the cavity.

All the multiplets are split with deformation qualitatively in the same way independent upon n and l. We should concentrate on the ordering with m of the single-particle orbits issued from the same spherical level. In the case of a prolate shape the levels are always ordered with increasing values of m as in first-order perturbation theory. The energies change smoothly with deformation and the spreading of each multiplet increases. On the contrary, the multiplets are spread for the oblate case into

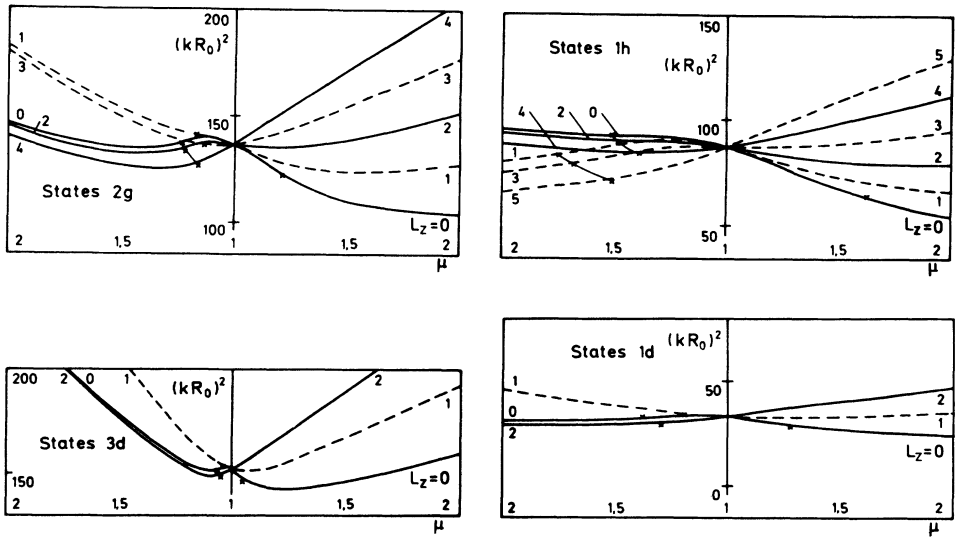

FIG. 6. Examples of splittings of single-particle orbits of a cavity with deformation (left: oblate, right: prolate) calculated in quantum mechanics. The cross or the arrows indicate solutions of Eqs. (77)—(79) of the text, i.e., the places where a given semiclassical state cross the separatrix: all the levels in the oblate case, only the level $L_z = 0$ in the prolate case.

TABLE I. For each component of the $1h$ multiplet labeled by L_z an oblate deformation has been calculated by solving Eqs. (77)—(79). They correspond to the places where the semiclassical levels cross the separatrix. The semiclassical energy levels E_{sc} are given altogether with the energy E_Q of the quantum state for these deformations. The relative errors are seen in the last column.

L_z	μ	$E_{sc}=(kR_0)^2_{sc}$	$E_Q=(kR_0)^2_Q$	$\Delta E/E_Q$
0	1.5118	91.785	92.754	1.05%
1	1.7461	82.687	83.769	1.29%
2	1.4858	89.745	90.720	1.07%
3	1.6821	78.944	80.075	1.41%
4	1.3898	83.554	84.531	1.15%
5	1.5024	71.309	72.667	1.87%

two components, for which m has an opposite parity. The lowest component is the one where m has the same parity as l. This is in exact agreement with what one expects from the semiclassical rule. The energy difference of levels of the same parity is constant within a very good approximation for a sufficiently large deformation, contrary to the expectation of first-order perturbation theory. The domain of perturbation theory is limited to small values of deformation only. We have indicated in Fig. 6 the place where the semiclassical eigenvalues cross the separatrix according to Eqs. (77), (78), and (79). By varying m continuously in these equations, one generates for given n and l two curves; the distance between these two curves and the behavior of the two groups of levels of opposite parity illustrates quite concretely the different slipping of the actions cells I_η and I_ξ that is experimented semiclassically. The difference between the quantum levels and the semiclassical eigenvalue is in the limit of 1%. This error has the same quality as that found for $m=0$ in Ref. 3. Notice that the uniform approximation is, as a matter of principle, mostly needed at the summit of the barrier. Therefore we can expect that the semiclassical description be generally of the same quality at least for other deformations. Table I provides a detailed comparison between the semiclassical value of $(kR_0)^2$ and its quantum equivalent for the deformation where the separatrix is found semiclassically.

In conclusion, it is possible to assert that the difference between spectra of oblate and prolate cavities is connected to the difference which exists between the phase spaces of classical trajectories. More simply, the richer spectrum for the oblate case is related to the existence of the focal circle.

IV. BUCK-PILT DIFFUSE POTENTIAL

A. Deformation of the diffuse potential

In Ref. 1 we have already studied semiclassically and quantum mechanically the spectrum of the spherical Buck-Pilt (or BP) potential[4] which is defined by

$$V(r)=-V_0\frac{1+\cosh(R_0/a)}{\cosh(r/a)+\cosh(R_0/a)} . \tag{81}$$

The parameter R_0 can be identified with the radius of the nucleus if $R_0=r_0A^{1/3}$ while a is the skin width. Throughout this paper we will use

$$V_0=52\text{ MeV},\quad \frac{R_0}{a}=11.517 . \tag{82}$$

This value of R_0 corresponds to $A=208$ if r_0 takes the value 1.2 fm.

Our aim is to connect the classical trajectories within such a potential to the quantum single-particle spectrum in the same way as for the cavity. The first step is to produce deformed equipotentials. Our choice was to produce them with ellipsoidal shape. The variable r is therefore replaced by the combination u of x, y, and z:

$$u=R_0\left[\frac{x^2+y^2}{R_\perp^2}+\frac{z^2}{R_z^2}\right]^{1/2} . \tag{83}$$

The deformation parameter is kept as $\mu=R_>/R_<=R_z/R_\perp$ (prolate) $=R_\perp/R_z$ (oblate) and the volume is conserved in such a way that

$$R_zR_\perp^2=R_0^3 . \tag{84}$$

The classical planar trajectories within such a potential were already studied by Carbonell[15] with particular emphasis on the case $R_0/a=4.89$ $(A=16)$ as well as $R_0/a=10.96$ $(A\approx208)$ and also with restriction on the prolate case. In this work the complexity of the phase space was already mentioned. In particular it was found that the deformed BP potential was not integrable; indeed chaotic trajectories were found for both values of R_0/a. A detailed description of the topological flow in phase space was provided and many bifurcations of periodic trajectories were studied as well as the conditions under which chaos occurred. This work was also partly discussed in Carbonell *et al.*[10]

In this paper we want to provide a description of the structure of phase space for nonplanar trajectories in comparison with the planar ones and we will study also prolate as well as oblate shapes. Our choice of R_0/a corresponds to the study of orbitals in heavy nuclei. Due to the large amount of work which was necessary, we have not studied the case of light nuclei.

There are two interesting limits which correspond to integrable potentials in which the phase-space structure is known. If $\mu\to1$, one obtains the spherical limit already studied in Ref. 1. If the excitation energy is small enough, the potential looks like a cavity with smooth edges. The energy is measured by the parameter η in terms of the absolute binding energy E' as

$$\eta=\frac{V_0-|E'|}{V_0} . \tag{85}$$

When $\eta\to1$ (and also if $\eta>1$), if $\mu\neq1$ the variation of the potential in the skin may play an important role for some trajectories and this variation brings about important nonlinear effects. It is reasonable to expect that these effects will be amplified if the trajectory stays a long time in the region where the potential changes the most. The destruction of tori in phase space, i.e., production of chaotic trajectories is then connected with the time passed

by the particle on the surface. On the contrary, trajectories confined mostly in regions where the potential is flat will stay on preserved tori. These remarks should be kept in mind if one looks at the results of Sec. IV B.

The questions developed from now on will be the following.

(i) What is the domain of the parameter space η, μ, and L_z where the phase-space structure can be understood mainly in terms of that of one of the integrable limits?

(ii) Where do the nonintegrable nonlinearities manifest themselves most strongly and in particular where does the macroscopic chaos occur?

B. Description of the phase space

The phase space is conveniently represented by drawing Poincaré surfaces of section[6,7] as function of various parameters. We have chosen the same representation as for the cavity, i.e., we select the intersection of the trajectories with the equatorial plane $z=0$ and we plot the successive values of the cylindrical coordinate ρ and p_ρ for various trajectories having the same value L_z, the same energy, and $p_z>0$. For $L_z\neq 0$ Poincaré surface of section is bounded by a trajectory entirely contained in the equatorial plane. This trajectory is itself contained by a trajectory located in the equatorial plane and having $L_z=0$. We have found it interesting to represent for every surface of section corresponding to $L_z\neq 0$ the boundary trajectory associated to this value as well as the one with $L_z=0$. The difference between these two curves measures the shrinking of phase space observed when the value of L_z is increased. This is the only scale effect which we have chosen to represent in our figures since ρ and p_ρ are always rescaled in such a way that their maximum value is a constant for every surface of section.

In order to simplify the notations the deformation parameter μ printed in the drawings of the Poincaré surface of section is $R_z/R_\perp$ so that values smaller than unity correspond to the oblate case. However when curves of energy levels are plotted, the definition $\mu=R_>/R_<$, more symmetric between prolate and oblate shapes, is preferred.

The value $\eta=0.625$ of the energy that is found most often in our figures is the energy at which lie the spherical eigenstate $1h$ for $A=208$. Since for this energy the sections are rather similar to those of the cavity, a few Poincaré sections are also provided for higher energies. There, because of higher nonlinearities, the structure of phase space does indeed change. The considerations of a situation adapted to a $1h$ level allows one also to draw conclusions about phase space which are large enough to accommodate several values of L_z, for example, from 0 to 5.

1. Prolate case

Figure 7 illustrates the simplest situation found for $L_z=3$ in the prolate case. The sections are made by in-

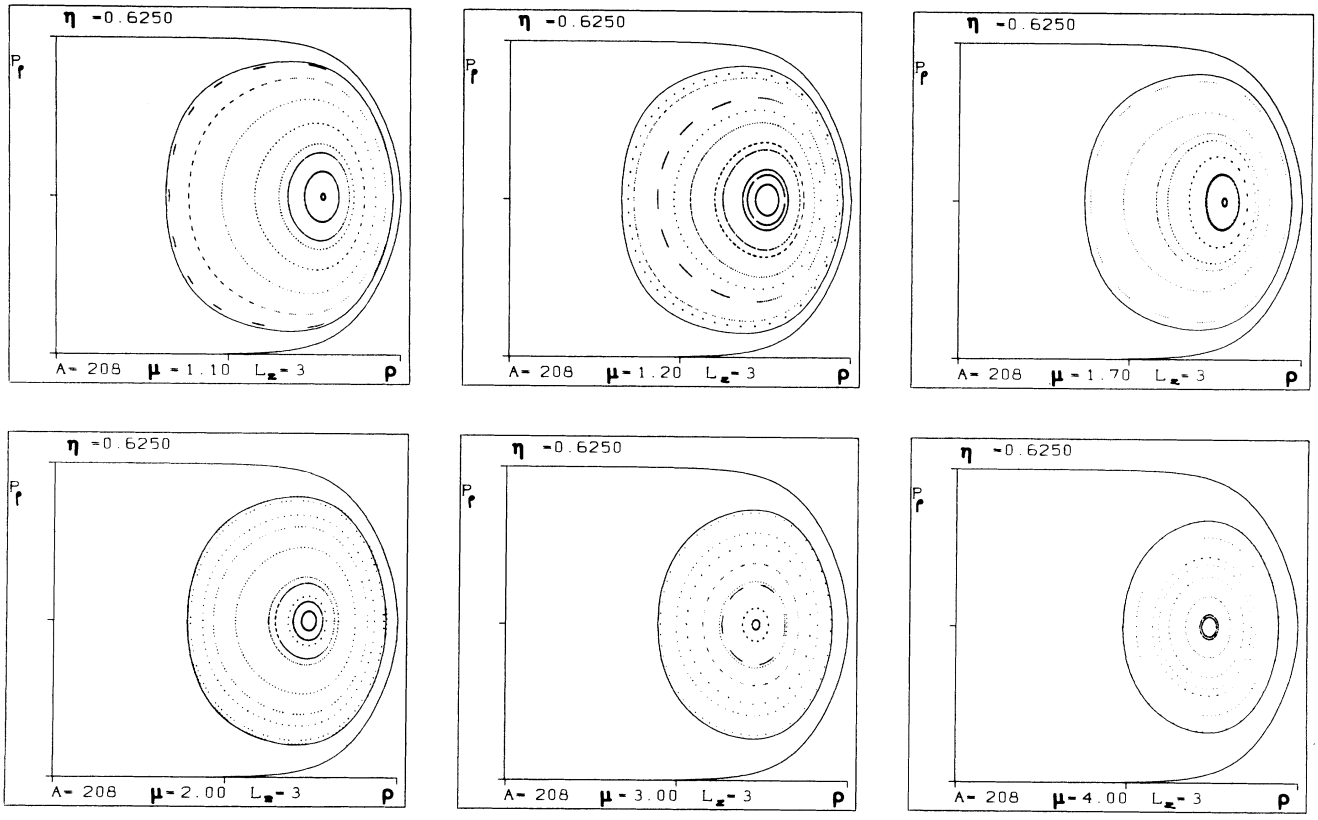

FIG. 7. Poincaré surfaces of section for the trajectories of a particle in a deformed prolate BP potential. The energy is labeled by η (here $\eta=0.625$ corresponds to the $1h$ level of ^{208}Pb). The deformation is $\mu=R_z/R_\perp$. For all these sections $L_z=3$. The outer boundary is that of the $L_z=0$ surface of section of the same η and μ. The fixed point in each section is a geodesiclike trajectory shown in Fig. 8. Note the similarity of these sections with Fig. 5(a).

variant curves which encircle a fixed point. This should be compared to Fig. 5(a) for the cavity where the fixed point corresponds to a geodesic of the ellipsoid. It is a remarkable result that the topology of Fig. 7 describes the same organization of the phase space. Indeed Fig. 8 represents in coordinates ρ and z two trajectories of the diffuse potential. One sees that the geodesic of the ellipsoid has an equivalent in the diffuse potential. This trajectory is the "skeleton" of the phase space for $L_z=3$, and all the other trajectories have in addition an oscillatory motion in the variable ϵ. There is no evidence at all, at least numerically, and for this resolution, that there is an appreciable change of structure of phase space for $L_z=3$ at this energy.

The effect of changing L_z for a fixed energy and deformation is shown in Fig. 9. There is no difference but a scale effect between $L_z=3$ and 5; the topology of the phase space is the same as in Fig. 1. On the other hand, the topology is entirely different for $L_z=0$ which corresponds well to a generic nonintegrable case. Chaotic trajectories are present as well as quasiperiodic ones. For $L_z=1$ the system looks nearer from an integrable case with the geodesiclike trajectory at the fixed point of the mapping. This drawing contains an important effect. When we consider high values of L_z, the trajectories are confined near the equatorial plane, i.e., in regions where the radius of curvature of the potential is slowly varying. On the other hand the trajectories with low L_z visit the totality of the potential. One can understand in this way why the nonlinearities play a more important role in the latter case.

Figure 10 shows the change with μ of the Poincaré sections for $L_z=0$. It provides the illustration of the transition toward chaos of a system which is integrable for $\mu=1$. The cases with $\mu=1.1$ and 1.2 present the two topologies found in the elliptical box and considered in Ref. 3. The fixed points of the mapping correspond to a trajectory homeomorphic to an ellipsis. According to a terminology first defined by Lord Rayleigh[16] which was used more recently in Ref. 17, this trajectory is the skeleton of the "whispering gallery" modes in an elliptical box. It is known that there are also the "bouncing ball" modes. The boundary of the surface of section of Fig. 9 which is a linear trajectory along the small axis of the ellipsoid belongs to this last category. This trajectory is stable in the BP potential for a broad interval of parameters. On the contrary there is another linear trajectory along the long axis, represented by the origin of coordinates, which is unstable. This instability produces the chaotic trajectories which are clearly visible already from $\mu=1.2$ on. Chaos originates from the separatrix between the two modes. It invades mainly the part of phase space where the whispering gallery trajectories were supposed to lie. Since the bouncing ball trajectories stand mostly in regions where the potential is smooth, they correspond to a part of phase space in which the tori are preserved much longer. Indeed even for $\mu=2$, tori are still found in this bouncing ball part. Islands have also been created; as usual in nonintegrable mappings, some of them are visible for $\mu=1.7$.

In Fig. 11 two larger values of η have been chosen: $\eta=0.8558$ which corresponds to the energy where the quantum $2g$ level is found for $\mu=1$ and $\eta=0.9231$ which corresponds to the energy of a $1j$ level. It is there clearly seen that chaos and nonintegrability are not a special property of $L_z=0$ only. Indeed the surface of section for $L_z=1$ shows a considerable change of structure. Very many islands have been created and their "interaction" can produce a visible macroscopic chaos. However for $L_z=3$ the structure of phase space is still the same as in Fig. 7. It is therefore a very important finding that the structure of phase space could change also very rapidly with L_z. The higher values of L_z correspond to a system closer to an integrable one.

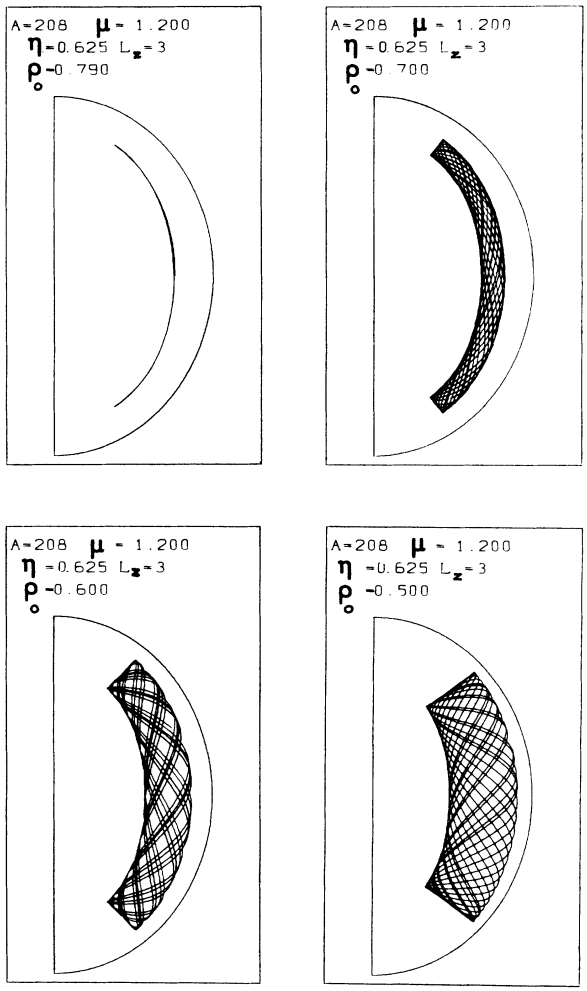

FIG. 8. Typical trajectories for a prolate BP potential with a $R_z/R_\perp=1.2$ deformation. The representation is the same as in Fig. 2. The upper-left trajectory is the geodesiclike. The value given for ρ_0 is the initial condition in the plane $z=0$.

2. *Oblate case*

Figures 12, 13, and 14 have been drawn in this case and can be compared, respectively, to Figs. 7, 9, and 10. In

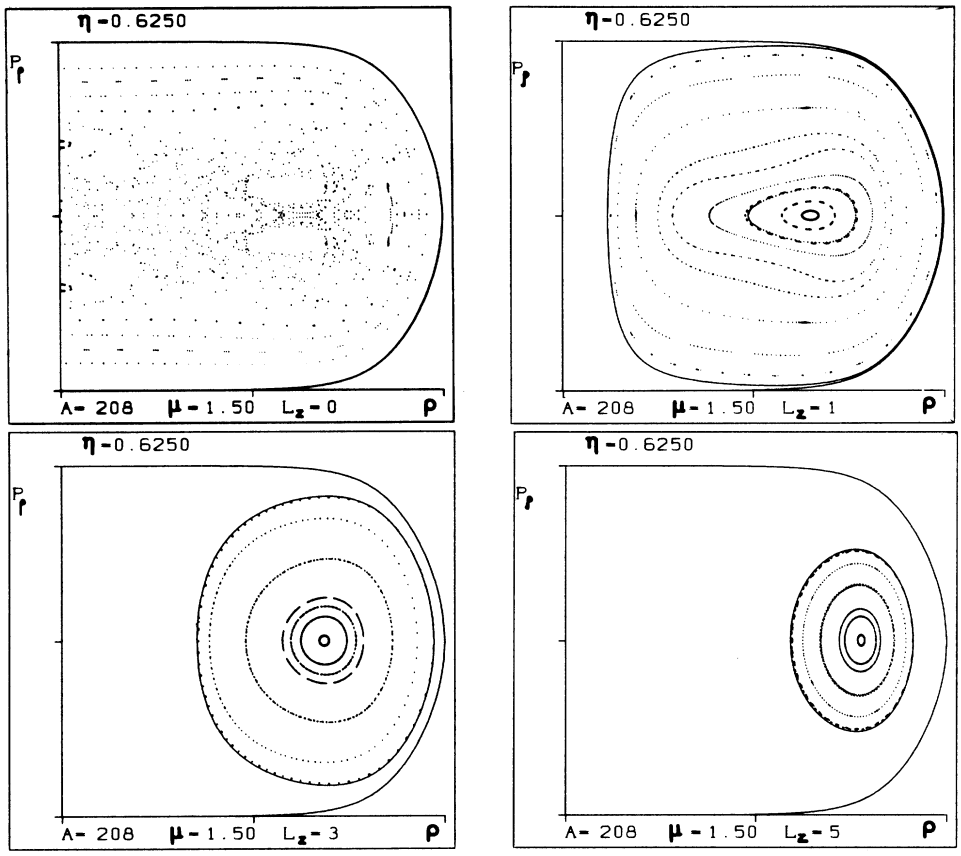

FIG. 9. Poincaré surfaces of section of a particle in a deformed prolate BP potential with $\eta=0.625$ and $\mu=1.5$ and $L_z=0,2\hbar,3\hbar,5\hbar$. Macroscopic chaos occurs only for $L_z=0$. The external boundary of each section is that for $L_z=0$.

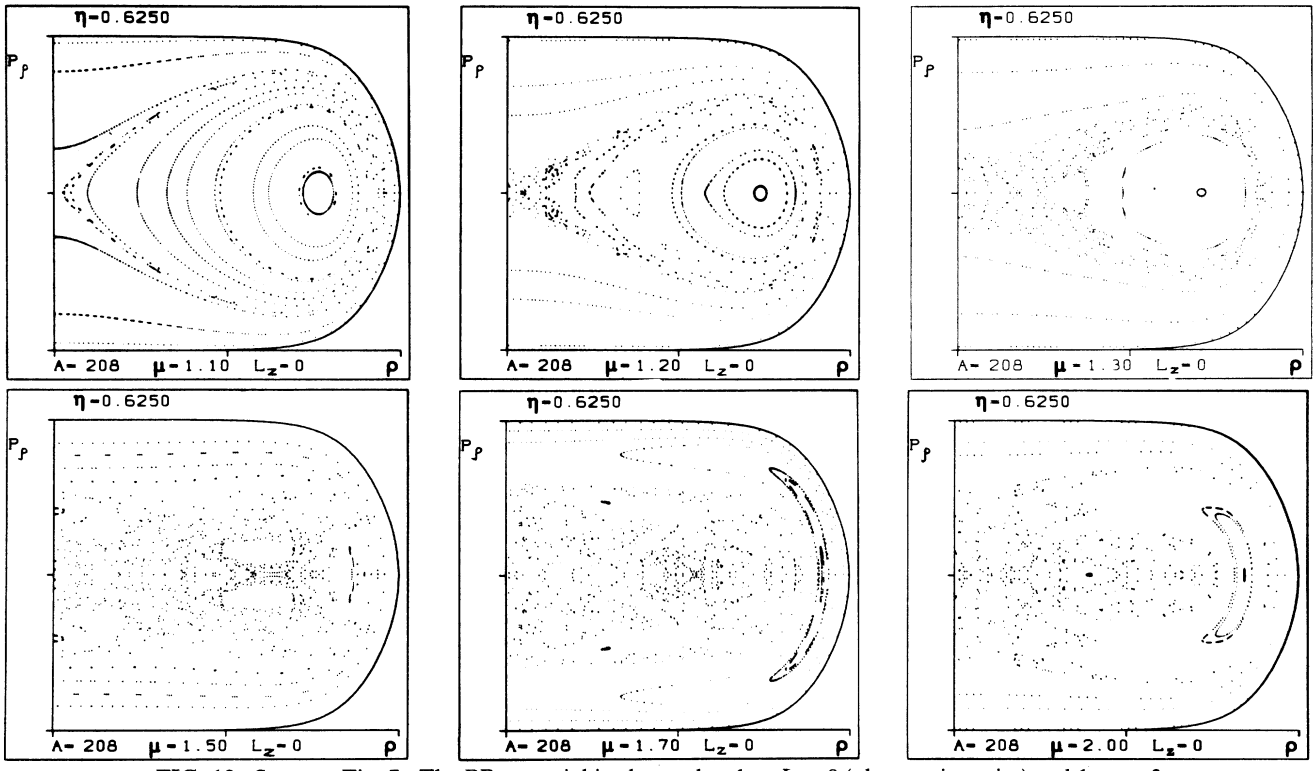

FIG. 10. Same as Fig. 7. The BP potential is also prolate but $L_z=0$ (plane trajectories) and $1<\mu\leq 2$.

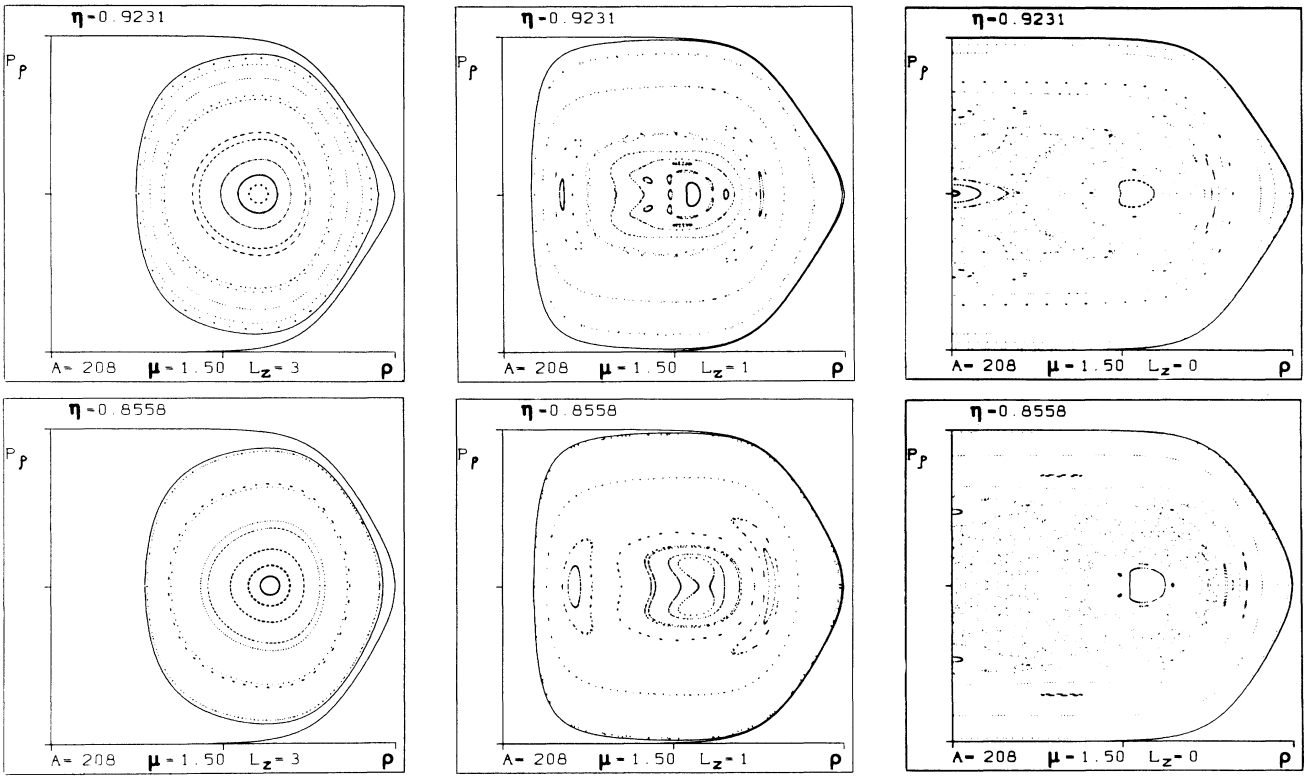

FIG. 11. Poincaré surfaces of section for a prolate BP potential for $L_z=0$, 1, and 3 and two energies: $\eta=0.8558$ (the $1g$ level of ^{208}Pb and $\eta=0.9321$ (the $1j$ level). $\mu=1.5$ everywhere.

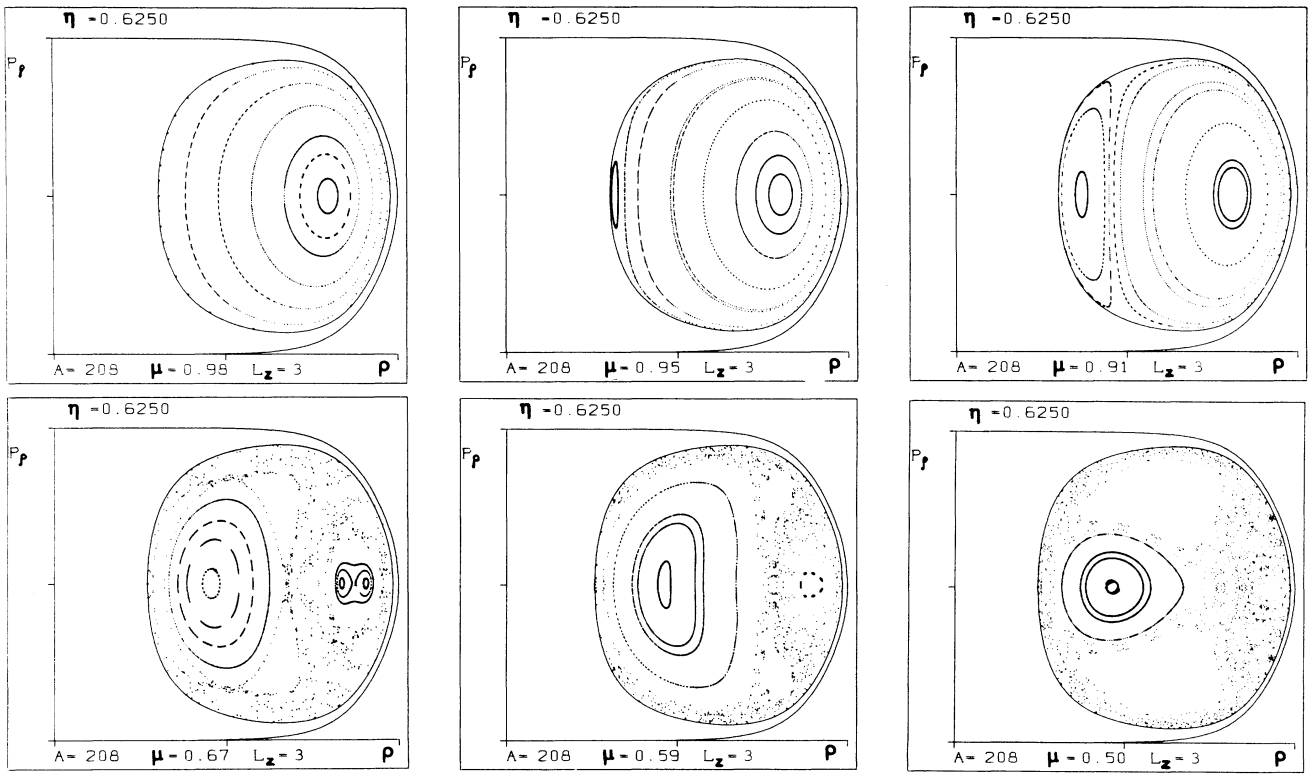

FIG. 12. Same as Fig. 7. The BP potential is now oblate and $L_z=3$. Its deformation, measured by $\mu=R_z/R_\perp$, is kept in a smaller interval as in Fig. 7 however. The first three sections are topologically equivalent to those of an oblate cavity [Figs. 5(b) and 5(c)]. Macroscopic chaos occurs now for $L_z=3$ at large deformation.

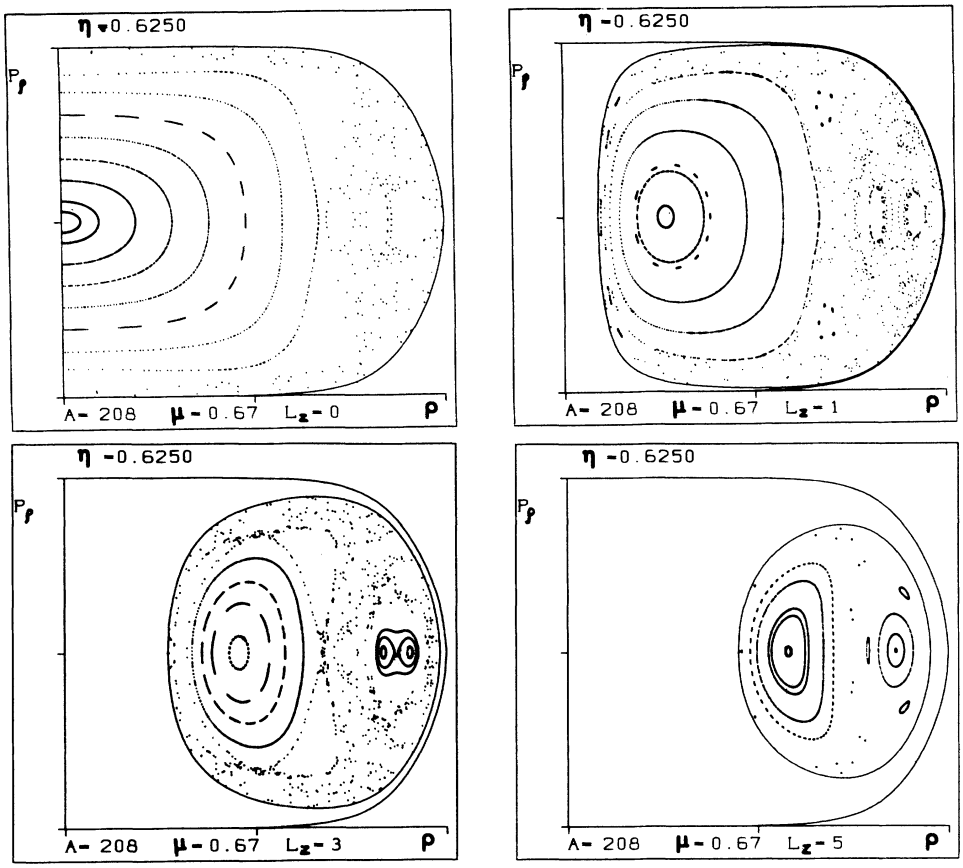

FIG. 13. Same as Fig. 9 but for an oblate BP potential. Note that we have here $R_z/R_\perp = 0.67 = 1/1.5$.

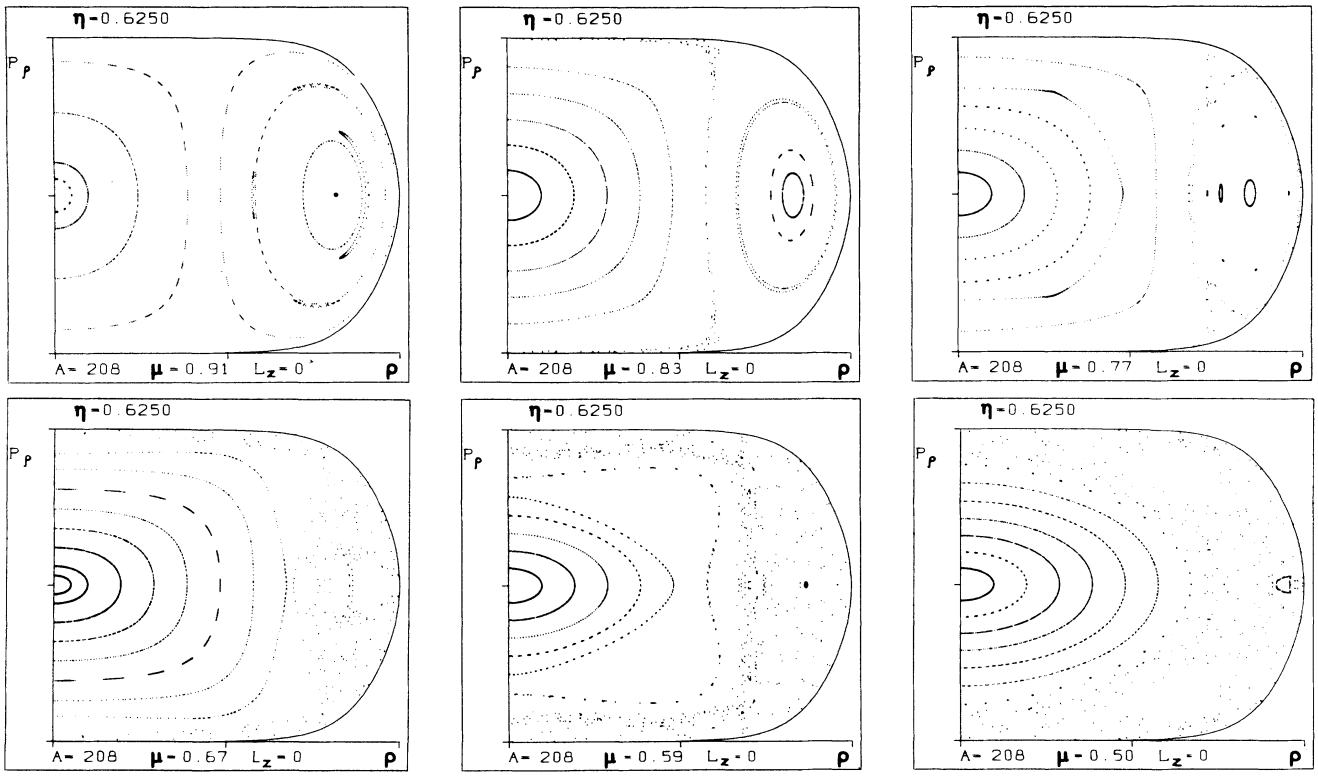

FIG. 14. Same as Fig. 10 but for an oblate BP potential.

the first three sections of Fig. 11 the phase-space structure for $L_z=3$ is topologically similar to that of the ellipsoidal oblate cavity. For small deformations the phase space is organized around a geodesiclike trajectory. When the deformation increases, a new part is created in phase space corresponding to a topology centered around the string binding a drumlike trajectory. This part of phase space becomes more important and is very stable. On the contrary, the former part decreases in size and becomes rapidly chaotic. This occurrence is similar to the situation of the $L_z=0$ trajectories in the prolate symmetry: Chaos invades first the region corresponding to the trajectories which visit most often the surface of the potential.

The difference between the values of L_z is less important than it was in the prolate case. In Fig. 13 we can see that the Poincaré section of $L_z=0$, 1, and 3 are qualitatively very similar. The linear trajectories along the small axis of the ellipsoid (the center of the section of $L_z=0$) is very stable and is surrounded by a large region occupied by invariant tori. On the contrary the whispering gallery modes are unstable and chaotic. It is seen that the $L_z=5$ curves still present some important stability around the geodesiclike trajectory.

The case with $L_z=0$ is studied in particular in Fig. 14 which should be compared to Fig. 10. It is interesting to notice that these figures represent the same topology (i.e., plane trajectories in a potential with equal values of $R_>/R_<$) but in the prolate case the Poincaré section is defined by the intersections with the small axis of the potential and in the oblate case by the interactions with the long axis. This is why the stability which occurs around the external part of the surface of section in Fig. 10 is transferred in Fig. 14 to the internal part. Notice that the potentials are nevertheless not exactly equivalent since the value of u associated with a given point by (83) depends on the symmetry of the potential oblate or prolate for the same value of $R_>/R_<$. Figure 15 completes the discussion about the stable bouncing ball-like trajectories and the unstable and chaotic trajectories around the boundary.

It is a remarkable result that the gross structure of the topology of the trajectories of the BP potential is still very similar to that of the cavity in spite of the disparity of the constants of motion. The increase of L_z weakens the nonlinear effects at the surface of the BP potential. This effect is more spectacular in the prolate case that in the oblate. In the latter case we have indeed the argument opposite to that given at the end of Sec. IV B 1. For high L_z the trajectories near the equatorial plane visit the surface at places where the radius of curvature is more rapidly varying. Hence chaos is created more easily for oblate shape than for prolate shape.

The analogy between the oblate BP potential and the cavity is underlined even more if one compares the trajectories of Fig. 16 to those of Fig. 14.

3. *Fine structure of the phase space*

The numerical exploration of the phase space which has been performed for the cavity provides, as is well known for other nonintegrable systems,[5–7] a coarse description which can be refined by enlarging the scale of the surfaces

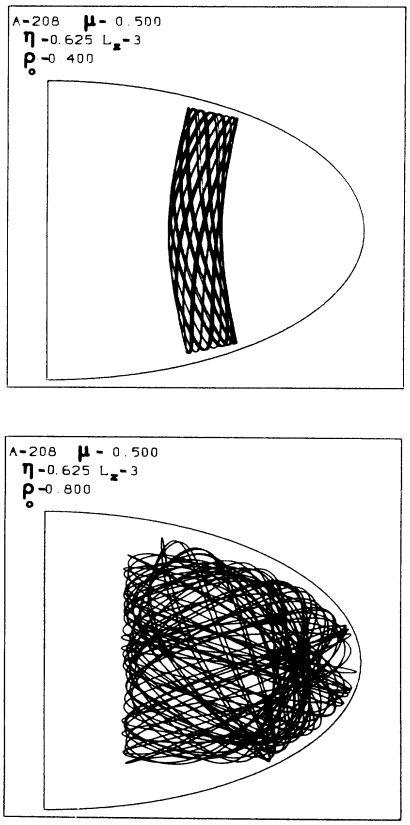

FIG. 15. Two trajectories are shown in an oblate BP potential with $R_z/R_\perp=0.5$ and $L_z=3$. The upper one is quasiperiodic; it is organized like the "string binding a drum" trajectory; the lower is chaotic. Both can be found in the bottom-right surface of section of Fig. 12.

of section and by calculating a larger number of trajectories. In this procedure the pictures of the phase space change and become highly complex. This event differentiates the phase space of a nonintegrable system from that of an integrable one.[7] The preceding discussion may lead the reader to the conclusion that the BP potential is integrable in a large region of deformation, energies, and values of L_z. This conclusion is totally wrong as shown in the example presented below.

In Fig. 17 we have drawn a surface of section for a prolate BP potential for $L_z=3$, $\eta=0.63$, and for an intermediate value of the deformation parameter $\mu=1.54$. We have also plotted, on each side, two periodic trajectories, with opposite curvature, which correspond to specific initial conditions. It is seen that a crescent-like structure occurs in the surface of section. At the center of the crescent is found the stable periodic trajectory found on the right on Fig. 17. At the opposite side with respect to the center of the Poincaré section is found the other (left-side) periodic trajectory which is seen to be unstable. The occurrence of such islands or resonances is of course well known.[8] It is a remarkable fact that we have found this structure by using the method of adiabatic switching developed in Refs. 19 and 20 and applied more recently by several authors.[18–21] Figure 17 shows such new topology,

which has no connection with the cavity for the more appropriate values of the parameters. The history of this topology, i.e., the place in energy where it is created, the other place eventually where it will bifurcate, or be destroyed, can be traced by using general methods about fixed points of mappings. These methods are, for example, described in Ref. 7. In our case one of us[9] has performed a detailed study of these islands for the $L_z=0$ trajectories. Indeed as we can see from Figs. 10 and 14 this is the place where the nonlinearities occur most easily. This work has not been repeated for the nonplanar trajectories discussed mainly in this paper.

The main reasons are the following. Such a work can be done by studying the properties of the Poincaré mappings, i.e., those of the isolated points of the mappings, their stability, or their bifurcations. For the planar trajec-

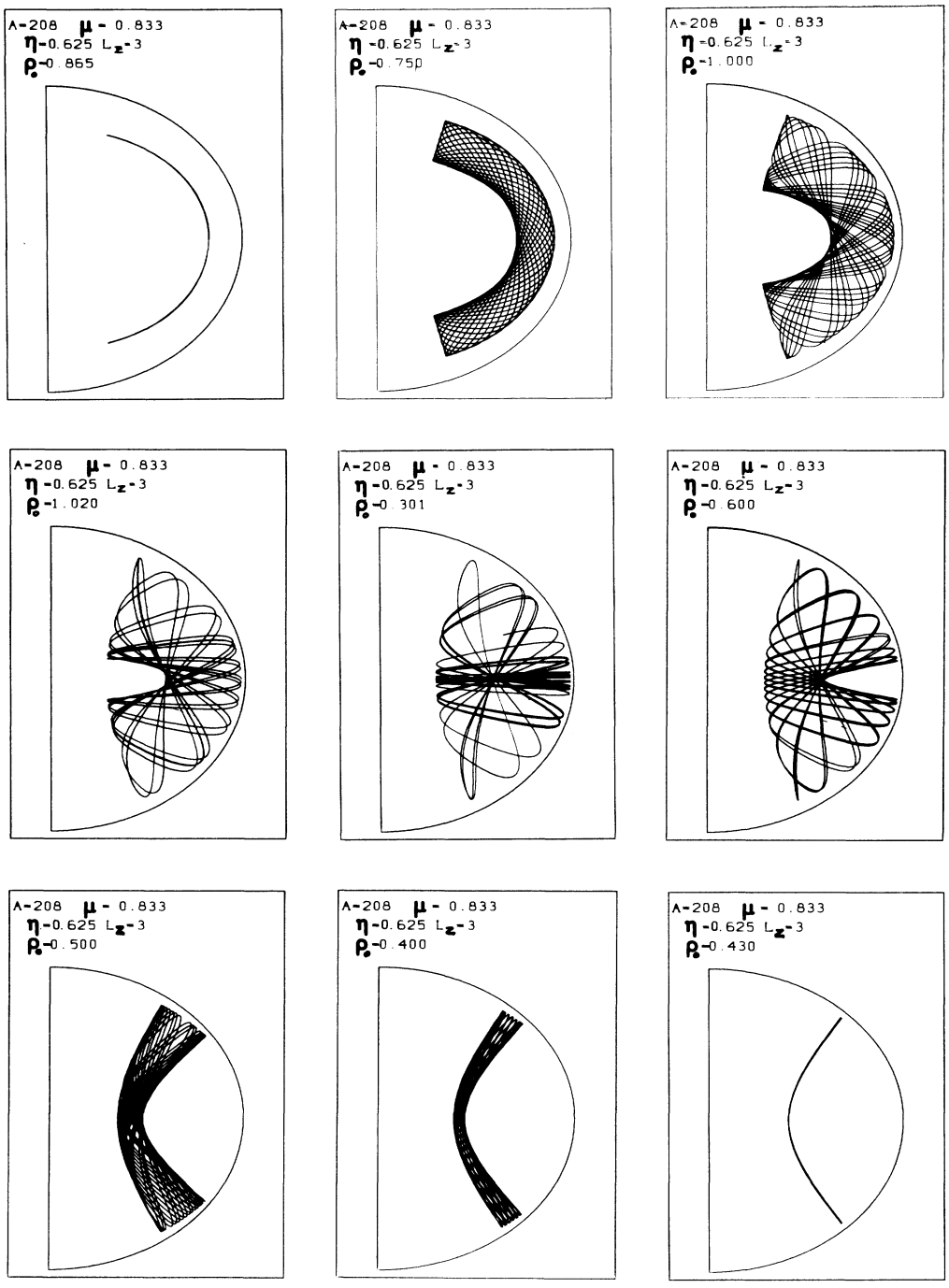

FIG. 16. Typical trajectories in an oblate BP potential with an oblate deformation of $R_z/R_\perp=0.833$. Here $L_z=3$ everywhere. The representation is the same as in Figs. 2, 4, and 8. The upper-left trajectory is the geodesiclike, the bottom-right, the "string binding a drum"-like.

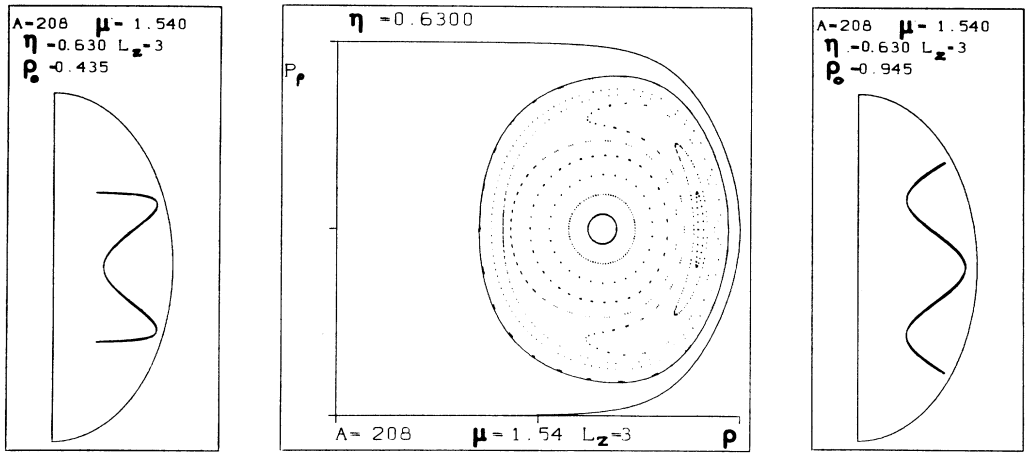

FIG. 17. A more careful drawing of Poincaré surfaces of section of a prolate BP potential for $\mu=1.54$, $\eta=0.63$, and $L_z=3$. A crescentlike structure occurs, which is not visible in Fig. 7. At the center of this structure one finds the curved trajectory shown on the right. This structure is stable. In a region where there is a higher density of points in the surface of section, one finds the unstable trajectory shown on the left part.

tories such trajectories are easily found. They are the linear motion along the small axis or the long axis of the potential.[9] From this study, important and visible effects are seen. On the contrary, for the mapping associated with the nonplanar trajectories the necessity to find out numerically the relevant periodic trajectories is a first difficulty. A second lies in the property that the nonlinearities of the mappings there are not so strong as for $L_z=0$ since the centrifugal barrier seems to smooth them out. Therefore most of the bifurcations produce a structure too small to be visible. As a matter of illustration we remind the reader that we have not been able to produce macroscopic chaotic trajectories for prolate shapes with $L_z=3$ and for values of μ as large as 4.

C. Quantum calculations

We have calculated the quantum single-particle energies for the BP deformed potential by diagonalization in a truncated deformed oscillator basis which includes 11 oscillator shells. A few deformed multiplets are drawn in Fig. 18 for comparison with their partners in the cavity. It is remarkable that the structure of the splittings is the same for both systems. For prolate deformation the energy levels are split as in perturbation theory: Even and odd L_z states are alternatively found with increasing energy. On the contrary, with the oblate symmetry the L_z states are grouped into two components: the even and the odd. The ordering of one family with respect to the other on

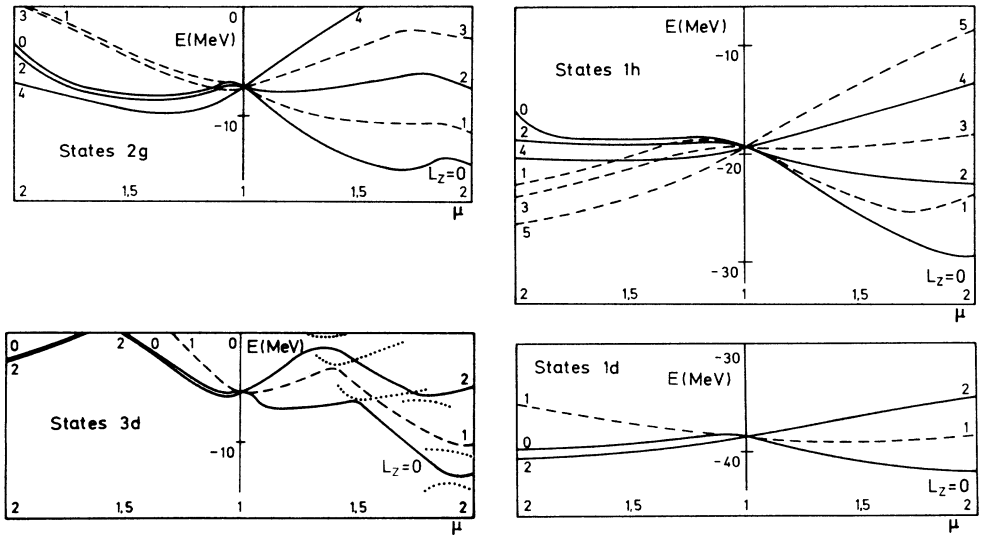

FIG. 18. Example of splittings of single-particle orbits of a deformed BP potential with a prolate (right) or oblate (left) deformation calculated in quantum mechanics. Some anticrossings are exhibited for the $3d$ case (they are not shown for other levels). Some Poincaré surfaces of section of the classical motion and some trajectories are shown in Figs. 7 to 17 for the unperturbed value $\eta=0.625$ of the $1h$ level. To be compared to Fig. 6.

the one hand and the ordering inside each component on the other hand are qualitatively identical with that explained in the case of the cavity. The only difference with the cavity lies in the crossings which occur in Fig. 18 and not in Fig. 6.

We can therefore estimate that the Schrödinger equation for a deformed BP potential can be separated in a reasonably good approximation in spheroidal coordinates and that the effective potential curves represented above form again the basis of the discussion of the spectrum. This remark as well as that given above for the crossings illustrates a discussion that has been given by Berry and Tabor[22] and by Berry.[23,24] On the scale of h^3 the individual levels can be located by a quantization condition. If the spectrum is observed with a finer scale, deviations occur like the noncrossing of the energy levels which are out of the range of a semiclassical description.

V. CONCLUSIONS

The aim of the preceding papers[1-3] and of the present one was first to obtain a description of the classical phase space corresponding to the motion of an independent nucleon, a neutron since Coulomb effects were not considered, in the average field of the nuclei. The different potentials that we have considered were either simply constant potentials—cavity, spherical, or deformed—all of them being integrable, and also diffuse spherical or deformed BP potentials. The spherical version of the latter is also integrable but the deformed one is nonintegrable. It is a current practice to teach nuclear physics and also to understand many physical effects by approximating the average field by an harmonic oscillator or an infinite box. The comparison is generally performed in a somewhat vague sense. We think that we have shown in our papers that a deeper connection can be found if one compares indeed the topology of the phase spaces of the simpler integrable potentials with those of the nonintegrable ones up to a certain resolution. Within that resolution the topologies are indeed identical. In the present paper we have emphasized that the properties of the ellipsoidal cavity explain those of the deformed BP potential, including the oblate-prolate difference, for a radius corresponding to heavy nucleus. In earlier papers[9,10] it was found in a similar fashion that for a radius corresponding to a light nucleus the phase space of a BP potential was topologically identical with that of an harmonic oscillator.

It is important to underline that the energy levels of these systems can nevertheless be different quantitatively. For example, those of the light nuclei can present some anharmonicities which can be understood properly in terms of the EBK approximation.[10] The semiclassical quantization method is a very powerful tool for separable systems like the cavity. In Ref. 3 we have indeed obtained extremely good spectra for the $L_z=0$ spectrum of a cavity using the uniform approximation. Such a method would probably provide results of the same quality for $L_z\neq 0$ as well. We have obtained a significant example in Table I in this direction. However, this method requires a considerable amount of time for a nonintegrable potential as we found[10] for the BP deformed potential with $L_z=0$. Another difficulty arises for the oblate case where the existence of a separatrix for the BP potential needs in addition to use a uniform approximation. Work in that direction using the adiabatic switching method[18-21,25,26] is in progress. At the present time we feel that the comparison between the integrable cavity and the nonintegrable BP potential stands only on the qualitative side.

In the present paper we feel that we have presented an interesting and new difference between prolate and oblate cavities that has a geometric origin in spite of our demonstration which used classical dynamics. It is very gratifying to observe that, starting from these explanations, one is able to trace also differences between the quantum-mechanical spectra not only of the cavity itself but also of the BP deformed potential.

We have also shown how the combination of deformation and surface diffuseness that is done in the BP potential is able to produce a classical macroscopic chaos. We reiterate here our conclusions regarding this production. Chaos is produced most easily in the phase space with low L_z; it requires oblate rather than prolate shapes and a rather small binding energy. Each of these conditions is one of the criteria upon which the nonlinearities are maximized. It is a rather surprising result that the phase space with high values of L_z correspond to lower nonlinearities. However it should be stressed that the preceding conditions are nevertheless not rare in nuclear physics. One knows indeed single-particle states of low binding energy with low L_z in largely deformed nuclei which can possibly correspond to a classical chaotic motion. These results give some additional support to the attempts to discover manifestation of quantum chaos in nuclear spectra.

We note that a great deal of effort has been provided in that field in the last recent years.[27] In particular Abdul Magd and Weidenmuller[27] have analyzed data on low-lying levels in nuclei ranging from ^{24}Na to ^{244}Am. They found indications for regularity in rotational-like states in even-even nuclei and also some evidence that natural parity states in odd-odd nuclei are not completely chaotic. On the other hand, the other states seem to have statistical distributions which are consistent with complete chaoticity. Obviously our results cannot be used directly to discuss these conclusions since we have been concerned only with the central part of the average potential. We feel that it would be an interesting work to find out how chaos and regular motion would appear in the coupling between the single particle and the collective degrees of freedom.

ACKNOWLEDGMENT

We would like to thank Y. Ayant for his collaboration during the work on the uniform approximation and the energy levels of the ellipsoidal cavity.

[1]J. Carbonell, F. Brut, R. Arvieu, and J. Touchard, J. Phys. G **11**, 385 (1985).
[2]Y. Ayant and R. Arvieu, J. Phys. A (to be published). Note that we have changed the variable η to ϵ.
[3]R. Arvieu and Y. Ayant, J. Phys. A (to be published).
[4]B. Buck and A. Pilt, Nucl. Phys. **A280**, 133 (1977).
[5]G. Contopoulos, Astron. J. **68**, 1 (1963).
[6]M. Henon and C. Heiles, Astron. J. **69**, 73 (1964).
[7]A. J. Lichtenberg and M. A. Lieberman, *Regular and Stochastic Motion* (Springer, New York, 1983).
[8]R. Arvieu, in *Phase Space Approach to Nuclear Dynamics,* Trieste meeting, edited by M. Di Toro, W. Nörenberg, M. Rosina, S. Stringari (World Scientific, Singapore 1986), p. 509.
[9]J. Carbonell, Thèse de 3ème cycle, Université de Grenoble, 1983.
[10]J. Carbonell, F. Brut, R. Arvieu, and J. Touchard, J. Phys. Paris Colloq. **45**, C6-371 (1984).
[11]V. M. Strutinsky, A. G. Magner, S. R. Ofengenden, and T. Dossing, Z. Phys. A **283**, 269 (1977).
[12]K. Helfrich, Theoret. Chim. Acta **24**, 271 (1972).
[13]H. A. Erikson and E. L. Hill, Phys. Rev. **75**, 29 (1949).
[14]H. Goldstein, *Classical Mechanics* (Addison-Wesley, Reading, MA, 1980).
[15]K. W. Ford, D. L. Hill, M. Wakano, and J. A. Wheeler, Ann. Phys. (N.Y.) **7**, 239 (1959).
[16]J. W. S. Rayleigh, *The Theory of Sound* (Dover, New York, 1945).
[17]J. B. Keller and S. I. Rubinow, Ann. Phys. (N.Y.) **9**, 24 (1960).
[18]B. R. Johnson, J. Chem. Phys. **82**, 4611 (1985).
[19]T. P. Grodzdanov, S. Saini, and H. S. Taylor, Phys. Rev. A **33**, 55 (1986).
[20]T. P. Grodzdanov, S. Saini, and H. S. Taylor, J. Chem. Phys. **84**, 3243 (1986).
[21]E. Cota, J. Flores, P. A. Mello, and E. Ypez, Phys. Lett. **53B**, 32 (1974).
[22]M. V. Berry and M. Tabor, Proc. R. Soc. London, Ser. A **356**, 375 (1977).
[23]M. V. Berry, *Chaotic Behavior in Quantum Systems,* edited by G. Casati (Plenum, New York, 1983).
[24]M. V. Berry (unpublished).
[25]O. Bohigas, M. J. Giannoni, and C. Schmidt, Phys. Rev. Lett. **52**, 1 (1984).
[26]T. H. Seligman, J. J. M. Verbaarschot, and H. A. Weidenmüller, Phys. Lett. **167B**, 365 (1986).
[27]A. Y. Abdul Magd and H. A. Weidenmüller, Phys. Lett. **162B**, 223 (1985).